

PAPER • OPEN ACCESS

Amplitude analysis of the decays $D^0 \rightarrow \pi^+ \pi^- \pi^+ \pi^-$ and $D^0 \rightarrow \pi^+ \pi^- \pi^0 \pi^0$

To cite this article: M. Ablikim *et al* 2024 *Chinese Phys. C* **48** 083001

View the [article online](#) for updates and enhancements.

You may also like

- [Search for Gravitational Waves Associated with Gamma-Ray Bursts Detected by Fermi and Swift during the LIGO–Virgo Run O3b](#)

R. Abbott, T. D. Abbott, F. Acernese et al.

- [Constraints from LIGO O3 Data on Gravitational-wave Emission Due to R-modes in the Glitching Pulsar PSR J0537-6910](#)

R. Abbott, T. D. Abbott, S. Abraham et al.

- [Search for Gravitational-lensing Signatures in the Full Third Observing Run of the LIGO–Virgo Network](#)

R. Abbott, H. Abe, F. Acernese et al.

Amplitude analysis of the decays $D^0 \rightarrow \pi^+ \pi^- \pi^+ \pi^-$ and $D^0 \rightarrow \pi^+ \pi^- \pi^0 \pi^{0*}$

M. Ablikim (麦迪娜)¹ M. N. Achasov^{4,c} P. Adlarson⁷⁵ O. Afedulidis³ X. C. Ai (艾小聰)⁸⁰ R. Aliberti³⁵
 A. Amoroso^{74A,74C} Q. An (安琪)^{71,58,a} Y. Bai (白羽)⁵⁷ O. Bakina³⁶ I. Balossino^{29A} Y. Ban (班勇)^{46,h}
 H.-R. Bao (包浩然)⁶³ V. Batozskaya^{1,44} K. Begzsuren³² N. Berger³⁵ M. Berlowski⁴⁴ M. Bertani^{28A} D. Bettini^{29A}
 F. Bianchi^{74A,74C} E. Bianco^{74A,74C} A. Bortone^{74A,74C} I. Boyko³⁶ R. A. Briere⁵ A. Brueggemann⁶⁸ H. Cai (蔡浩)⁷⁶
 X. Cai (蔡嘯)^{1,58} A. Calcaterra^{28A} G. F. Cao (曹国富)^{1,63} N. Cao (曹宁)^{1,63} S. A. Cetin^{62A} J. F. Chang (常劲帆)^{1,58}
 W. L. Chang^{1,63} G. R. Che (车国荣)⁴³ G. Chelkov^{36,b} C. Chen (陈琛)⁴³ C. H. Chen (陈春卉)⁹ Chao Chen (陈超)⁵⁵
 G. Chen (陈刚)¹ H. S. Chen (陈和生)^{1,63} M. L. Chen (陈玛丽)^{1,58,63} S. J. Chen (陈申见)⁴² S. L. Chen (陈思璐)⁴⁵
 S. M. Chen (陈少敏)⁶¹ T. Chen (陈通)^{1,63} X. R. Chen (陈旭荣)^{31,63} X. T. Chen (陈肖婷)^{1,63} Y. B. Chen (陈元柏)^{1,58}
 Y. Q. Chen³⁴ Z. J. Chen (陈卓俊)^{25,i} Z. Y. Chen (陈正元)^{1,63} S. K. Choi¹⁰ X. Chu⁴³ G. Cibinetto^{29A} F. Cossio^{74C}
 J. J. Cui (崔佳佳)⁵⁰ H. L. Dai (代洪亮)^{1,58} J. P. Dai (代建平)⁷⁸ A. Dbeysi¹⁸ R. E. de Boer³ D. Dedovich³⁶
 C. Q. Deng (邓创旗)⁷² Z. Y. Deng (邓子艳)¹ A. Denig³⁵ I. Denysenko³⁶ M. Destefanis^{74A,74C} F. De Mori^{74A,74C}
 B. Ding (丁彪)^{66,1} X. X. Ding (丁晓萱)^{46,h} Y. Ding (丁逸)³⁴ Y. Ding (丁勇)⁴⁰ J. Dong (董静)^{1,58}
 L. Y. Dong (董燎原)^{1,63} M. Y. Dong (董明义)^{1,58,63} X. Dong (董翔)⁷⁶ M. C. Du (杜蒙川)¹ S. X. Du (杜书先)⁸⁰
 Z. H. Duan (段宗欢)⁴² P. Egorov^{36,b} Y. H. Fan (范宇晗)⁴⁵ J. Fang (方建)^{1,58} J. Fang (方进)⁵⁹ S. S. Fang (房双世)^{1,63}
 W. X. Fang (方文兴)¹ Y. Fang (方易)¹ Y. Q. Fang (方亚泉)^{1,58} R. Farinelli^{29A} L. Fava^{74B,74C} F. Feldbauer³
 G. Felici^{28A} C. Q. Feng (封常青)^{71,58} J. H. Feng (冯俊华)⁵⁹ Y. T. Feng (冯筠潼)^{71,58} K. Fischer⁶⁹ M. Fritsch³
 C. D. Fu (傅成栋)¹ J. L. Fu (傅金林)⁶³ Y. W. Fu (傅亦威)^{1,63} H. Gao (高涵)⁶³ Y. N. Gao (高原宁)^{46,h}
 Yang Gao (高扬)^{71,58} S. Garbolino^{74C} I. Garzia^{29A,29B} P. T. Ge (葛潘婷)⁷⁶ Z. W. Ge (葛振武)⁴² C. Geng (耿聪)⁵⁹
 E. M. Gersabeck⁶⁷ A. Gilman⁶⁹ K. Goetzen¹³ L. Gong (龚丽)⁴⁰ W. X. Gong (龚文煊)^{1,58} W. Gradl³⁵
 S. Gramigna^{29A,29B} M. Greco^{74A,74C} M. H. Gu (顾旻皓)^{1,58} Y. T. Gu (顾运厅)¹⁵ C. Y. Guan (关春懿)^{1,63}
 Z. L. Guan²² A. Q. Guo (郭爱强)^{31,63} L. B. Guo (郭立波)⁴¹ M. J. Guo (国梦娇)⁵⁰ R. P. Guo (郭如盼)⁴⁹
 Y. P. Guo (郭玉萍)^{12,f} A. Guskov^{36,b} J. Gutierrez²⁷ K. L. Han (韩坤霖)⁶³ T. T. Han (韩婷婷)¹ X. Q. Hao (郝喜庆)¹⁹
 F. A. Harris⁶⁵ K. K. He (何凯凯)⁵⁵ K. L. He (何康林)^{1,63} F. H. Heinsius³ C. H. Heinz³⁵ Y. K. Heng (衡月昆)^{1,58,63}
 C. Herold⁶⁰ T. Holtmann³ P. C. Hong^{12,f} G. Y. Hou (侯国一)^{1,63} X. T. Hou (侯贤涛)^{1,63} Y. R. Hou (侯颖锐)⁶³
 Z. L. Hou (侯治龙)¹ B. Y. Hu (胡碧颖)⁵⁹ H. M. Hu (胡海明)^{1,63} J. F. Hu (胡继峰)^{56,j} T. Hu (胡涛)^{1,58,63}
 Y. Hu (胡誉)¹ G. S. Huang (黄光顺)^{71,58} K. X. Huang (黄凯旋)⁵⁹ L. Q. Huang (黄麟钦)^{31,63} X. T. Huang (黄性涛)⁵⁰
 Y. P. Huang (黄燕萍)¹ T. Hussain⁷³ F. H"olzken³ N. H"usken^{27,35} N. in der Wiesche⁶⁸ M. Irshad^{71,58} J. Jackson²⁷
 S. Janchiv³² J. H. Jeong¹⁰ Q. Ji (纪全)¹ Q. P. Ji (姬清平)¹⁹ W. Ji (季旺)^{1,63} X. B. Ji (季晓斌)^{1,63}
 X. L. Ji (季筱璐)^{1,58} Y. Y. Ji (吉钰瑶)⁵⁰ X. Q. Jia (贾晓倩)⁵⁰ Z. K. Jia (贾泽坤)^{71,58} D. Jiang (姜地)^{1,63}
 H. B. Jiang (姜候兵)⁷⁶ P. C. Jiang (蒋沛成)^{46,h} S. S. Jiang (姜赛赛)³⁹ T. J. Jiang (蒋庭俊)¹⁶ X. S. Jiang (江晓山)^{1,58,63}

Received 6 December 2023; Accepted 10 April 2024; Published online 11 April 2024

* Supported in part by the National Key R&D Program of China (2020YFA0406300, 2020YFA0406400); the National Natural Science Foundation of China (NSFC) (11625523, 11635010, 11735014, 11835012, 11935015, 11935016, 11935018, 11961141012, 12025502, 12035009, 12035013, 12061131003, 12105276, 12122509, 12192260, 12192261, 12192262, 12192263, 12192264, 12221005, 12225509, 12235017); the Chinese Academy of Sciences (CAS) Large-Scale Scientific Facility Program; the CAS Center for Excellence in Particle Physics (CCEPP); Joint Large-Scale Scientific Facility Funds of the NSFC and CAS (U1732263, U1832103, U1832207, U2032111); CAS Key Research Program of Frontier Sciences (QYZDJ-SSW-SLH003, QYZDJ-SSW-SLH040); 100 Talents Program of CAS; The Institute of Nuclear and Particle Physics (INPAC) and Shanghai Key Laboratory for Particle Physics and Cosmology; European Union's Horizon 2020 research and innovation programme under Marie Skłodowska-Curie grant agreement (894790); German Research Foundation DFG (455635585); Collaborative Research Center CRC 1044, FOR5327, GRK 2149; Istituto Nazionale di Fisica Nucleare, Italy; Ministry of Development of Turkey (DPT2006K-120470); National Research Foundation of Korea (NRF-2022R1A2C1092335); National Science and Technology fund of Mongolia; National Science Research and Innovation Fund (NSRF) via the Program Management Unit for Human Resources & Institutional Development, Research and Innovation of Thailand (B16F640076); Polish National Science Centre (2019/35/O/ST2/02907); The Swedish Research Council; U. S. Department of Energy (DE-FG02-05ER41374)

 Content from this work may be used under the terms of the Creative Commons Attribution 3.0 licence. Any further distribution of this work must maintain attribution to the author(s) and the title of the work, journal citation and DOI. Article funded by SCOAP³ and published under licence by Chinese Physical Society and the Institute of High Energy Physics of the Chinese Academy of Sciences and the Institute of Modern Physics of the Chinese Academy of Sciences and IOP Publishing Ltd

- Y. Jiang (蒋艺)⁶³ J. B. Jiao (焦健斌)⁵⁰ J. K. Jiao (焦俊坤)³⁴ Z. Jiao (焦铮)²³ S. Jin (金山)⁴² Y. Jin (金毅)⁶⁶
 M. Q. Jing (荆茂强)^{1,63} X. M. Jing (景新媚)⁶³ T. Johansson⁷⁵ S. Kabana³³ N. Kalantar-Nayestanaki⁶⁴
 X. L. Kang (康晓琳)⁹ X. S. Kang (康晓珅)⁴⁰ M. Kavatsyuk⁶⁴ B. C. Ke (柯百谦)⁸⁰ V. Khachatryan²⁷ A. Khoukaz⁶⁸
 R. Kiuchi¹ O. B. Kolcu^{62A} B. Kopf⁸ M. Kuessner³ X. Kui (奎贤)^{1,63} A. Kupsc^{44,75} W. Kl"uhn³⁷ J. J. Lane⁶⁷
 P. Larin¹⁸ L. Lavezzi^{74A,74C} T. T. Lei (雷天天)^{71,58} Z. H. Lei (雷祚弘)^{71,58} H. Leithoff⁸⁵ M. Lellmann³⁵ T. Lenz³⁵
 C. Li (李翠)⁴⁷ C. Li (李聪)⁴³ C. H. Li (李春花)³⁹ Cheng Li (李澄)^{71,58} D. M. Li (李德民)⁸⁰ F. Li (李飞)^{1,58}
 G. Li (李刚)¹ H. Li^{71,58} H. B. Li (李海波)^{1,63} H. J. Li (李惠静)¹⁹ H. N. Li (李衡讷)^{56,j} Hui Li (李慧)⁴³
 J. R. Li (李嘉荣)⁶¹ J. S. Li (李静舒)⁵⁹ K. Li (李科)¹ L. J. Li (李林健)^{1,63} L. K. Li (李龙科)¹ Lei Li (李蕾)⁴⁸
 M. H. Li (李明浩)⁴³ P. R. Li (李培荣)^{38,k,l} Q. M. Li (李启铭)^{1,63} Q. X. Li (李起鑫)⁵⁰ R. Li (李燃)^{17,31}
 S. X. Li (李素娴)¹² T. Li (李腾)⁵⁰ W. D. Li (李卫东)^{1,63} W. G. Li (李卫国)^{1,a} X. Li (李旭)^{1,63} X. H. Li (李旭红)^{71,58}
 X. L. Li (李晓玲)⁵⁰ X. Y. Li (李晓宇)^{1,63} Y. G. Li (李彦谷)^{46,h} Z. J. Li (李志军)⁵⁹ Z. X. Li (李振轩)¹⁵
 C. Liang (梁畅)⁴² H. Liang (梁昊)^{71,58} H. Liang (梁浩)^{1,63} Y. F. Liang (梁勇飞)⁵⁴ Y. T. Liang (梁羽铁)^{31,63}
 G. R. Liao (廖广睿)¹⁴ L. Z. Liao (廖龙洲)⁵⁰ Y. P. Liao (廖一朴)^{1,63} J. Libby²⁶ A. Limphirat⁶⁰
 D. X. Lin (林德旭)^{31,63} T. Lin (林韬)¹ B. J. Liu (刘北江)¹ B. X. Liu (刘宝鑫)⁷⁶ C. Liu (刘成)³⁴ C. X. Liu (刘春秀)¹
 F. Liu (刘芳)¹ F. H. Liu (刘福虎)⁵³ Feng Liu (刘峰)⁶ G. M. Liu (刘国明)^{56,j} H. Liu (刘昊)^{38,k,l}
 H. B. Liu (刘宏邦)¹⁵ H. H. Liu (刘欢欢)¹ H. M. Liu (刘怀民)^{1,63} Huihui Liu (刘汇慧)²¹ J. B. Liu (刘建北)^{71,58}
 J. Y. Liu (刘晶译)^{1,63} K. Liu (刘凯)^{38,k,l} K. Y. Liu (刘魁勇)⁴⁰ Ke Liu (刘珂)²² L. Liu (刘亮)^{71,58}
 L. C. Liu (刘良辰)⁴³ Lu Liu (刘露)⁴³ M. H. Liu (刘美宏)^{12,g} P. L. Liu (刘佩莲)¹ Q. Liu (刘倩)⁶³
 S. B. Liu (刘树彬)^{71,58} T. Liu (刘桐)^{12,g} W. K. Liu (刘维克)⁴³ W. M. Liu (刘卫民)^{71,58} X. Liu (刘鑫)³⁹
 X. Liu (刘翔)^{38,k,l} Y. Liu (刘义)⁸⁰ Y. Liu (刘英)^{38,k,l} Y. B. Liu (刘玉斌)⁴³ Z. A. Liu (刘振安)^{1,58,63}
 Z. D. Liu (刘宗德)⁹ Z. Q. Liu (刘智青)⁵⁰ X. C. Lou (娄辛丑)^{1,58,63} F. X. Lu (卢飞翔)⁵⁹ H. J. Lu (吕海江)²³
 J. G. Lu (吕军光)^{1,58} X. L. Lu (陆小玲)¹ Y. Lu (卢宇)⁷ Y. P. Lu (卢云鹏)^{1,58} Z. H. Lu (卢泽辉)^{1,63}
 C. L. Luo (罗成林)⁴¹ M. X. Luo (罗民兴)⁷⁹ T. Luo (罗涛)^{12,g} X. L. Luo (罗小兰)^{1,58} X. R. Lyu (吕晓睿)⁶³
 Y. F. Lyu (吕翌丰)⁴³ F. C. Ma (马凤才)⁴⁰ H. Ma (马衡)⁷⁸ H. L. Ma (马海龙)¹ J. L. Ma (马俊力)^{1,63}
 L. L. Ma (马连良)⁵⁰ M. M. Ma (马明明)^{1,63} Q. M. Ma (马秋梅)¹ R. Q. Ma (马润秋)^{1,63} X. T. Ma (马晓天)^{1,63}
 X. Y. Ma (马骁妍)^{1,58} Y. Ma^{46,g} Y. M. Ma (马玉明)³¹ F. E. Maas¹⁸ M. Maggiora^{74A,74C} S. Malde⁶⁹ A. Mangoni^{28B}
 Y. J. Mao (冒亚军)^{46,h} Z. P. Mao (毛泽普)¹ S. Marcelli^{74A,74C} Z. X. Meng (孟召霞)⁶⁶ J. G. Messchendorp^{13,64}
 G. Mezzadri^{29A} H. Miao (妙晗)^{1,63} T. J. Min (闵天觉)⁴² R. E. Mitchell²⁷ X. H. Mo (莫晓虎)^{1,58,63} B. Moses²⁷
 N. Yu. Muchnoi^{4,c} J. Muskalla³⁵ Y. Nefedov³⁶ F. Nerling^{18,e} I. B. Nikolaev^{4,c} Z. Ning (宁哲)^{1,58} S. Nisar^{11,m}
 Q. L. Niu (牛祺乐)^{38,k,l} W. D. Niu (牛文迪)⁵⁵ Y. Niu (牛艳)⁵⁰ S. L. Olsen⁶³ Q. Ouyang (欧阳群)^{1,58,63}
 S. Pacetti^{28B,28C} X. Pan (潘祥)⁵⁵ Y. Pan (潘越)⁵⁷ A. Pathak³⁴ P. Patteri^{28A} Y. P. Pei (裴宇鹏)^{71,58} M. Pelizaeus³
 H. P. Peng (彭海平)^{71,58} Y. Y. Peng (彭云翊)^{38,k,l} K. Peters^{13,e} J. L. Ping (平加伦)⁴¹ R. G. Ping (平荣刚)^{1,63}
 S. Plura³⁵ V. Prasad³³ F. Z. Qi (齐法制)¹ H. Qi (齐航)^{71,58} H. R. Qi (漆红荣)⁶¹ M. Qi (祁鸣)⁴²
 T. Y. Qi (齐天钰)^{12,g} S. Qian (钱森)^{1,58} W. B. Qian (钱文斌)⁶³ C. F. Qiao (乔从丰)⁶³ J. J. Qin (秦佳佳)⁷²
 L. Q. Qin (秦丽清)¹⁴ X. S. Qin (秦小帅)⁵⁰ Z. H. Qin (秦中华)^{1,58} J. F. Qiu (邱进发)¹ S. Q. Qu (屈三强)⁶¹
 Z. H. Qu (屈子皓)⁷² C. F. Redmer³⁵ K. J. Ren (任旷洁)³⁹ A. Rivetti^{74C} M. Rolo^{74C} G. Rong (荣刚)^{1,63}
 Ch. Rosner¹⁸ S. N. Ruan (阮氏宁)⁴³ N. Salone⁴⁴ A. Sarantsev^{36,d} Y. Schelhaas³⁵ K. Schoenning⁷⁵
 M. Scodeggio^{29A} K. Y. Shan (尚科羽)^{12,g} W. Shan (单葳)²⁴ X. Y. Shan (单心钰)^{71,58} J. F. Shangguan (上官剑锋)¹⁶
 L. G. Shao (邵立港)^{1,63} M. Shao (邵明)^{71,58} C. P. Shen (沈成平)^{12,g} H. F. Shen (沈宏飞)^{1,8} W. H. Shen (沈文涵)⁶³
 X. Y. Shen (沈肖雁)^{1,63} B. A. Shi (施伯安)⁶³ H. C. Shi (石煌超)^{71,58} J. L. Shi (石家磊)^{12,g} J. Y. Shi (石京燕)¹
 Q. Q. Shi (石勤强)⁵⁵ R. S. Shi^{1,63} S. Y. Shi (史书宇)⁷² X. Shi (史欣)^{1,58} X. D. Shi (师晓东)^{71,58}
 J. J. Song (宋娇娇)¹⁹ T. Z. Song (宋天资)⁵⁹ W. M. Song (宋维民)^{34,1} Y. J. Song (宋宇镜)¹² Y. X. Song (宋匀轩)^{46,g,m}
 S. Sosio^{74A,74C} S. Spataro^{74A,74C} F. Stieler³⁵ Y. J. Su (粟杨捷)⁶³ G. B. Sun (孙光豹)⁷⁶ G. X. Sun (孙功星)¹
 H. Sun (孙昊)⁶³ H. K. Sun (孙浩凯)¹ J. F. Sun (孙俊峰)¹⁹ K. Sun (孙开)⁶¹ L. Sun (孙亮)⁷⁶ S. S. Sun (孙胜森)^{1,63}
 T. Sun^{51,f} W. Y. Sun (孙文玉)³⁴ Y. Sun (孙源)⁹ Y. J. Sun (孙勇杰)^{71,58} Y. Z. Sun (孙永昭)¹ Z. Q. Sun (孙泽群)^{1,63}
 Z. T. Sun (孙振田)⁵⁰ C. J. Tang (唐昌建)⁵⁴ G. Y. Tang (唐光毅)¹ J. Tang (唐健)⁵⁹ Y. A. Tang (唐迎澳)⁷⁶

- L. Y. Tao (陶璐燕)⁷² Q. T. Tao (陶秋田)^{25,i} M. Tat⁶⁹ J. X. Teng (滕佳秀)^{71,58} V. Thoren⁷⁵ W. H. Tian (田文辉)⁵⁹
Y. Tian (田野)^{31,63} Z. F. Tian (田喆飞)⁷⁶ I. Uman^{62B} Y. Wan (万宇)⁵⁵ S. J. Wang (王少杰)⁵⁰ B. Wang (王斌)¹
B. L. Wang (王滨龙)⁶³ Bo Wang (王博)^{71,58} D. Y. Wang (王大勇)^{46,h} F. Wang (王菲)⁷² H. J. Wang (王泓鉴)^{38,k,l}
J. P. Wang (王吉鹏)⁵⁰ K. Wang (王科)^{1,58} L. L. Wang (王亮亮)¹ M. Wang (王萌)⁵⁰ Meng Wang^{1,63}
N. Y. Wang (王南洋)⁶³ S. Wang (王顺)^{12,g} S. Wang (王石)^{38,k,l} T. Wang (王婷)^{12,g} T. J. Wang (王腾蛟)⁴³
W. Wang (王为)⁵⁹ W. Wang (王维)⁷² W. P. Wang (王维平)^{35,58,71} X. Wang (王轩)^{46,h} X. F. Wang (王雄飞)^{38,k,l}
X. J. Wang (王希俊)³⁹ X. L. Wang (王小龙)^{12,g} X. N. Wang (王新南)¹ Y. Wang (王亦)⁶¹ Y. D. Wang (王雅迪)⁴⁵
Y. F. Wang (王贻芳)^{1,58,63} Y. L. Wang (王艺龙)¹⁹ Y. N. Wang (王亚男)⁴⁵ Y. Q. Wang (王雨晴)¹
Yaqian Wang (王亚乾)¹⁷ Yi Wang (王义)⁶¹ Z. Wang (王铮)^{1,58} Z. L. Wang (王治浪)⁷² Z. Y. Wang (王至勇)^{1,63}
Ziyi Wang (王子一)⁶³ D. Wei⁷⁰ D. H. Wei (魏代会)¹⁴ F. Weidner⁶⁸ S. P. Wen (文硕频)¹ Y. R. Wen (温亚冉)³⁹
U. Wiedner³ G. Wilkinson⁶⁹ M. Wolke⁷⁵ L. Wollenberg³ C. Wu (吴晨)³⁹ J. F. Wu (吴金飞)^{1,8}
L. H. Wu (伍灵慧)¹ L. J. Wu (吴连近)^{1,63} X. Wu (吴潇)^{12,g} X. H. Wu (伍雄浩)³⁴ Y. Wu (吴言)^{71,58}
Y. H. Wu (吴业昊)⁵⁵ Y. J. Wu (吴英杰)³¹ Z. Wu (吴智)^{1,58} L. Xia (夏磊)^{71,58} X. M. Xian (咸秀梅)³⁹
B. H. Xiang (向本后)^{1,63} T. Xiang (相腾)^{46,h} D. Xiao (肖栋)^{38,k,l} G. Y. Xiao (肖光延)⁴² S. Y. Xiao (肖素玉)¹
Y. L. Xiao (肖云龙)^{12,g} Z. J. Xiao (肖振军)⁴¹ C. Xie (谢陈)⁴² X. H. Xie (谢昕海)^{46,h} Y. Xie (谢勇)⁵⁰
Y. G. Xie (谢宇广)^{1,58} Y. H. Xie (谢跃红)⁶ Z. P. Xie (谢智鹏)^{71,58} T. Y. Xing (邢天宇)^{1,63} C. F. Xu^{1,63}
C. J. Xu (许创杰)⁵⁹ G. F. Xu (许国发)¹ H. Y. Xu (许皓月)^{66,2} Q. J. Xu (徐庆君)¹⁶ Q. N. Xu³⁰ W. Xu (许威)¹
W. L. Xu (徐万伦)⁶⁶ X. P. Xu (徐新平)⁵⁵ Y. C. Xu (胥英超)⁷⁷ Z. P. Xu (许泽鹏)⁴² Z. S. Xu (许昭燊)⁶³
F. Yan (严芳)^{12,g} L. Yan (严亮)^{12,g} W. B. Yan (鄢文标)^{71,58} W. C. Yan (闫文成)⁸⁰ X. Q. Yan (严薛强)^{1,63}
H. J. Yang (杨海军)^{51,f} H. L. Yang (杨昊霖)³⁴ H. X. Yang (杨洪勋)¹ T. Yang (杨涛)¹ Y. Yang (杨莹)^{12,g}
Y. F. Yang (杨翊凡)^{1,63} Y. F. Yang (杨艳芳)⁴³ Y. X. Yang (杨逸翔)^{1,63} Z. W. Yang (杨政武)^{38,k,l}
Z. P. Yao (姚志鹏)⁵⁰ M. Ye (叶梅)^{1,58} M. H. Ye (叶铭汉)⁸ J. H. Yin (殷俊昊)¹ Z. Y. You (尤郑昀)⁵⁹
B. X. Yu (俞伯祥)^{1,58,63} C. X. Yu (喻纯旭)⁴³ G. Yu (余刚)^{1,63} J. S. Yu (俞洁晟)^{25,i} T. Yu (于涛)⁷²
X. D. Yu (余旭东)^{46,h} C. Z. Yuan (苑长征)^{1,63} J. Yuan (袁菁)³⁴ L. Yuan (袁丽)² S. C. Yuan (苑思成)^{1,63}
Y. Yuan (袁野)^{1,63} Z. Y. Yuan (袁朝阳)⁵⁹ C. X. Yue (岳崇兴)³⁹ A. A. Zafar⁷³ F. R. Zeng (曾凡蕊)⁵⁰
S. H. Zeng (曾胜辉)⁷² X. Zeng (曾鑫)^{12,g} Y. Zeng (曾云)^{25,i} Y. J. Zeng (曾溢嘉)^{1,63} Y. J. Zeng (曾宇杰)⁵⁹
X. Y. Zhai (翟星晔)³⁴ Y. C. Zhai (翟云聪)⁵⁰ Y. H. Zhan (詹永华)⁵⁹ A. Q. Zhang (张安庆)^{1,63}
B. L. Zhang (张伯伦)^{1,63} B. X. Zhang (张丙新)¹ D. H. Zhang (张丹昊)⁴³ G. Y. Zhang (张广义)¹⁹
H. Zhang (张豪)^{71,58} H. C. Zhang (张航畅)^{1,58,63} H. H. Zhang (张宏浩)⁵⁹ H. H. Zhang (张宏宏)³⁴
H. Q. Zhang (张华桥)^{1,58,63} H. Y. Zhang (章红宇)^{1,58} J. Zhang (张进)⁸⁰ J. Zhang (张晋)⁵⁹ J. J. Zhang (张进军)⁵²
J. L. Zhang (张杰磊)²⁰ J. Q. Zhang (张敬庆)⁴¹ J. W. Zhang (张家文)^{1,58,63} J. X. Zhang (张景旭)^{38,j,k}
J. Y. Zhang (张建勇)¹ J. Z. Zhang (张景芝)^{1,63} Jianyu Zhang (张剑宇)⁶³ L. M. Zhang (张黎明)⁶¹ Lei Zhang (张雷)⁴²
P. Zhang (张鹏)^{1,63} Q. Y. Zhang^{39,80} S. H. Zhang (张水涵)^{1,63} Shulei Zhang (张书磊)^{25,i} X. D. Zhang (张小东)⁴⁵
X. M. Zhang (张晓梅)¹ X. Y. Zhang (张学尧)⁵⁰ Y. Zhang (张宇)⁷² Y. Zhang (张瑶)¹ Y. T. Zhang (张亚腾)⁸⁰
Y. H. Zhang (张银鸿)^{1,58} Y. M. Zhang (张悦明)³⁹ Yan Zhang (张言)^{71,58} Z. D. Zhang (张正德)¹
Z. H. Zhang (张泽恒)¹ Z. L. Zhang (张兆领)³⁴ Z. Y. Zhang (张子羽)⁴³ Z. Y. Zhang (张振宇)⁷⁶ G. Zhao (赵光)¹
J. Y. Zhao (赵静宜)^{1,63} J. Z. Zhao (赵京周)^{1,58} L. Zhao (赵玲)¹ Lei Zhao (赵雷)^{71,58} M. G. Zhao (赵明刚)⁴³
R. P. Zhao (赵若平)⁶³ S. J. Zhao (赵书俊)⁸⁰ Y. B. Zhao (赵豫斌)^{1,58} Y. X. Zhao (赵宇翔)^{31,63}
Z. G. Zhao (赵政国)^{71,58} A. Zhemchugov^{36,b} B. Zheng (郑波)⁷² J. P. Zheng (郑建平)^{1,58} W. J. Zheng (郑文静)^{1,63}
Y. H. Zheng (郑阳恒)⁶³ B. Zhong (钟彬)⁴¹ X. Zhong (钟鑫)⁵⁹ H. Zhou (周航)⁵⁰ J. Y. Zhou (周佳莹)³⁴
L. P. Zhou (周利鹏)^{1,63} X. Zhou (周详)⁷⁶ X. K. Zhou (周晓康)⁶ X. R. Zhou (周小蓉)^{71,58} X. Y. Zhou (周兴玉)³⁹
Y. Z. Zhou (周袆卓)^{12,g} J. Zhu (朱江)⁴³ K. Zhu (朱凯)¹ K. J. Zhu (朱科军)^{1,58,63} L. Zhu (朱林)³⁴
L. X. Zhu (朱琳萱)⁶³ S. H. Zhu (朱世海)⁷⁰ S. Q. Zhu (朱仕强)⁴² T. J. Zhu (朱腾蛟)^{12,g} W. D. Zhu (朱稳定)⁴¹
Y. C. Zhu (朱莹春)^{71,58} Z. A. Zhu (朱自安)^{1,63} J. H. Zou (邹佳恒)¹ J. Zu (祖健)^{71,58}
- (BESIII Collaboration)

¹Institute of High Energy Physics, Chinese Academy of Sciences, Beijing 100049, China²Beihang University, Beijing 100191, China

- ³Bochum Ruhr-University, D-44780 Bochum, Germany
⁴Budker Institute of Nuclear Physics SB RAS (BINP), Novosibirsk 630090, Russia
⁵Carnegie Mellon University, Pittsburgh, Pennsylvania 15213, USA
⁶Central China Normal University, Wuhan 430079, China
⁷Central South University, Changsha 410083, China
⁸China Center of Advanced Science and Technology, Beijing 100190, China
⁹China University of Geosciences, Wuhan 430074, China
¹⁰Chung-Ang University, Seoul, 06974, Republic of Korea
¹¹COMSATS University Islamabad, Lahore Campus, Defence Road, Off Raiwind Road, 54000 Lahore, Pakistan
¹²Fudan University, Shanghai 200433, China
¹³GSI Helmholtzcentre for Heavy Ion Research GmbH, D-64291 Darmstadt, Germany
¹⁴Guangxi Normal University, Guilin 541004, China
¹⁵Guangxi University, Nanning 530004, China
¹⁶Hangzhou Normal University, Hangzhou 310036, China
¹⁷Hebei University, Baoding 071002, China
¹⁸Helmholtz Institute Mainz, Staudinger Weg 18, D-55099 Mainz, Germany
¹⁹Henan Normal University, Xinxiang 453007, China
²⁰Henan University, Kaifeng 475004, China
²¹Henan University of Science and Technology, Luoyang 471003, China
²²Henan University of Technology, Zhengzhou 450001, China
²³Huangshan College, Huangshan 245000, China
²⁴Hunan Normal University, Changsha 410081, China
²⁵Hunan University, Changsha 410082, China
²⁶Indian Institute of Technology Madras, Chennai 600036, India
²⁷Indiana University, Bloomington, Indiana 47405, USA
^{28A}INFN Laboratori Nazionali di Frascati, INFN Laboratori Nazionali di Frascati, I-00044, Frascati, Italy
^{28B}INFN Laboratori Nazionali di Frascati, INFN Sezione di Perugia, I-06100, Perugia, Italy
^{28C}INFN Laboratori Nazionali di Frascati, University of Perugia, I-06100, Perugia, Italy
^{29A}INFN Sezione di Ferrara, INFN Sezione di Ferrara, I-44122, Ferrara, Italy
^{29B}INFN Sezione di Ferrara, University of Ferrara, I-44122, Ferrara, Italy
³⁰Inner Mongolia University, Hohhot 010021, China
³¹Institute of Modern Physics, Lanzhou 730000, China
³²Institute of Physics and Technology, Peace Avenue 54B, Ulaanbaatar 13330, Mongolia
³³Instituto de Alta Investigaci\'on, Universidad de Tarapac\'a, Casilla 7D, Arica 1000000, Chile
³⁴Jilin University, Changchun 130012, China
³⁵Johannes Gutenberg University of Mainz, Johann-Joachim-Becher-Weg 45, D-55099 Mainz, Germany
³⁶Joint Institute for Nuclear Research, 141980 Dubna, Moscow region, Russia
³⁷Justus-Liebig-Universitaet Giessen, II. Physikalisches Institut, Heinrich-Buff-Ring 16, D-35392 Giessen, Germany
³⁸Lanzhou University, Lanzhou 730000, China
³⁹Liaoning Normal University, Dalian 116029, China
⁴⁰Liaoning University, Shenyang 110036, China
⁴¹Nanjing Normal University, Nanjing 210023, China
⁴²Nanjing University, Nanjing 210093, China
⁴³Nankai University, Tianjin 300071, China
⁴⁴National Centre for Nuclear Research, Warsaw 02-093, Poland
⁴⁵North China Electric Power University, Beijing 102206, China
⁴⁶Peking University, Beijing 100871, China
⁴⁷Qufu Normal University, Qufu 273165, China
⁴⁸Renmin University of China, Beijing 100872, China
⁴⁹Shandong Normal University, Jinan 250014, China
⁵⁰Shandong University, Jinan 250100, China
⁵¹Shanghai Jiao Tong University, Shanghai 200240, China
⁵²Shanxi Normal University, Linfen 041004, China
⁵³Shanxi University, Taiyuan 030006, China
⁵⁴Sichuan University, Chengdu 610064, China
⁵⁵Soochow University, Suzhou 215006, China
⁵⁶South China Normal University, Guangzhou 510006, China
⁵⁷Southeast University, Nanjing 211100, China
⁵⁸State Key Laboratory of Particle Detection and Electronics, Beijing 100049, Hefei 230026, China
⁵⁹Sun Yat-Sen University, Guangzhou 510275, China
⁶⁰Suranaree University of Technology, University Avenue 111, Nakhon Ratchasima 30000, Thailand
⁶¹Tsinghua University, Beijing 100084, China
^{62A}Turkish Accelerator Center Particle Factory Group, Istinye University, 34010, Istanbul, Turkey
^{62B}Turkish Accelerator Center Particle Factory Group, Near East University, Nicosia, North Cyprus, 99138, Mersin 10, Turkey
⁶³University of Chinese Academy of Sciences, Beijing 100049, China
⁶⁴University of Groningen, NL-9747 AA Groningen, The Netherlands
⁶⁵University of Hawaii, Honolulu, Hawaii 96822, USA
⁶⁶University of Jinan, Jinan 250022, China

⁶⁷University of Manchester, Oxford Road, Manchester, M13 9PL, United Kingdom⁶⁸University of Muenster, Wilhelm-Klemm-Strasse 9, 48149 Muenster, Germany⁶⁹University of Oxford, Keble Road, Oxford OX1 3RH, United Kingdom⁷⁰University of Science and Technology Liaoning, Anshan 114051, China⁷¹University of Science and Technology of China, Hefei 230026, China⁷²University of South China, Hengyang 421001, China⁷³University of the Punjab, Lahore-54590, Pakistan^{74A}University of Turin and INFN, University of Turin, I-10125, Turin, Italy^{74B}University of Turin and INFN, University of Eastern Piedmont, I-15121, Alessandria, Italy^{74C}University of Turin and INFN, INFN, I-10125, Turin, Italy⁷⁵Uppsala University, Box 516, SE-75120 Uppsala, Sweden⁷⁶Wuhan University, Wuhan 430072, China⁷⁷Yantai University, Yantai 264005, China⁷⁸Yunnan University, Kunming 650500, China⁷⁹Zhejiang University, Hangzhou 310027, China⁸⁰Zhengzhou University, Zhengzhou 450001, China^aAlso at the Moscow Institute of Physics and Technology, Moscow 141700, Russia^bAlso at the Novosibirsk State University, Novosibirsk, 630090, Russia^cAlso at the NRC "Kurchatov Institute", PNPI, 188300, Gatchina, Russia^dAlso at Goethe University Frankfurt, 60323 Frankfurt am Main, Germany^eAlso at Key Laboratory for Particle Physics, Astrophysics and Cosmology, Ministry of Education; Shanghai Key Laboratory for Particle Physics and Cosmology; Institute of Nuclear and Particle Physics, Shanghai 200240, China^fAlso at Key Laboratory of Nuclear Physics and Ion-beam Application (MOE) and Institute of Modern Physics, Fudan University, Shanghai 200443, China^gAlso at State Key Laboratory of Nuclear Physics and Technology, Peking University, Beijing 100871, China^hAlso at School of Physics and Electronics, Hunan University, Changsha 410082, ChinaⁱAlso at Guangdong Provincial Key Laboratory of Nuclear Science, Institute of Quantum Matter, South China Normal University, Guangzhou 510006, China^jAlso at MOE Frontiers Science Center for Rare Isotopes, Lanzhou University, Lanzhou 730000, China^kAlso at Lanzhou Center for Theoretical Physics, Lanzhou University, Lanzhou 730000, China^lAlso at the Department of Mathematical Sciences, IBA, Karachi 75270, Pakistan^mAlso at Ecole Polytechnique Federale de Lausanne (EPFL), CH-1015 Lausanne, Switzerland

Abstract: Using e^+e^- annihilation data corresponding to an integrated luminosity of 2.93 fb^{-1} taken at the center-of-mass energy $\sqrt{s} = 3.773 \text{ GeV}$ with the BESIII detector, a joint amplitude analysis is performed on the decays $D^0 \rightarrow \pi^+\pi^-\pi^+\pi^-$ and $D^0 \rightarrow \pi^+\pi^-\pi^0\pi^0(\text{non-}\eta)$. The fit fractions of individual components are obtained, and large interferences among the dominant components of the decays $D^0 \rightarrow a_1(1260)\pi$, $D^0 \rightarrow \pi(1300)\pi$, $D^0 \rightarrow \rho(770)\rho(770)$, and $D^0 \rightarrow 2(\pi\pi)_S$ are observed in both channels. With the obtained amplitude model, the CP -even fractions of $D^0 \rightarrow \pi^+\pi^-\pi^+\pi^-$ and $D^0 \rightarrow \pi^+\pi^-\pi^0\pi^0(\text{non-}\eta)$ are determined to be $(75.2 \pm 1.1_{\text{stat.}} \pm 1.5_{\text{syst.}}) \%$ and $(68.9 \pm 1.5_{\text{stat.}} \pm 2.4_{\text{syst.}}) \%$, respectively. The branching fractions of $D^0 \rightarrow \pi^+\pi^-\pi^+\pi^-$ and $D^0 \rightarrow \pi^+\pi^-\pi^0\pi^0(\text{non-}\eta)$ are measured to be $(0.688 \pm 0.010_{\text{stat.}} \pm 0.010_{\text{syst.}}) \%$ and $(0.951 \pm 0.025_{\text{stat.}} \pm 0.021_{\text{syst.}}) \%$, respectively. The amplitude analysis provides an important model for the binning strategy in measuring the strong phase parameters of $D^0 \rightarrow 4\pi$ when used to determine the CKM angle $\gamma(\phi_3)$ via the $B^- \rightarrow DK^-$ decay.

Keywords: BESIII, D^0 meson decays, amplitude analysis, CP -even fraction

DOI: 10.1088/1674-1137/ad3d4d

I. INTRODUCTION

Precision measurements of the elements of the Cabibbo-Kobayashi-Maskawa (CKM) matrix and the test of the unitarity of the CKM triangle [1, 2] are essential goals in the field of flavor physics. One of the three angles of the unitarity triangle, $\gamma(\phi_3) \equiv \arg(-V_{ud}V_{ub}^*/V_{cd}V_{cb}^*)$, can be measured with the tree-level decay $B^\pm \rightarrow DK^\pm$ through the interference between the $B^- \rightarrow D^0 K^-$ ($b \rightarrow c\bar{s}$) and $B^- \rightarrow \bar{D}^0 K^-$ ($b \rightarrow u\bar{s}$) amplitudes, which is one of the most important measurements of LHCb and Belle II. Several approaches have been proposed to measure the CKM angle γ via the decay $B^\pm \rightarrow DK^\pm$ [3–5].

Here, the relative magnitude and phase between the D^0 and \bar{D}^0 mesons decay into the same final states, and the D^0 decay parameters (*e.g.* CP -even fraction F_+) are the critical inputs. With more data collected by the LHCb and Belle II experiments in the future, the decay parameters of D^0 (\bar{D}^0) will become the dominant source of uncertainty in the γ measurement. Therefore, precision measurements of the D^0 decay parameters are urgently required to improve the precision of the γ measurement.

The decay $D^0 \rightarrow 4\pi$ is regarded as a sensitive mode [6, 7] to extract the CKM angle γ via $B^- \rightarrow DK^-$. Their CP -even fractions (F_+) and relatively strong phase parameters in the different phase space (PHSP) bins (c_i/s_i)

serve as the direct inputs in the GLW [3] and BPGGSZ [5, 8] methods, respectively. A reliable decay amplitude model of $D^0 \rightarrow 4\pi$ is critical to precisely extract F_+ and a model-independent c_i/s_i [6], and to search for CP violation in $D^0 \rightarrow 4\pi$ [9]. Moreover, the four-body D^0 hadronic decays provide an excellent platform to study the two-body decays $D^0 \rightarrow VV$ and $D^0 \rightarrow AP$, where V , A , and P denote vector, axial-vector, and pseudo-scalar mesons, respectively. These decays thus enhance the understanding of the decay dynamics of the D^0 meson [10, 11].

Currently, the experimental studies of $D^0 \rightarrow 4\pi$ are limited. The FOCUS experiment performed an amplitude analysis of $D^0 \rightarrow \pi^+\pi^-\pi^+\pi^-$ based on ~ 6000 candidate events with a background fraction of $\sim 10\%$ [12]. An amplitude analysis of $D^0 \rightarrow \pi^+\pi^-\pi^+\pi^-$ was also conducted with the CLEO-c data containing ~ 7000 candidate events with a background fraction of $\sim 20\%$ [13]. However, no amplitude analysis of $D^0 \rightarrow \pi^+\pi^-\pi^0\pi^0$ has been performed yet. BESIII has collected 2.93 fb^{-1} of e^+e^- collision data at the center-of-mass energy $\sqrt{s} = 3.773 \text{ GeV}$, where the $D\bar{D}$ pair is produced without any additional hadrons. This data sample provides an ideal environment for studying D meson decays with the double tag (DT) technique [14, 15]. In this method, a single tag (ST) candidate requires that only one D meson is reconstructed via the ST mode. A DT candidate requires that D and \bar{D} are reconstructed via the signal and ST modes, respectively. Based on this data sample and the DT method with three ST modes $\bar{D}^0 \rightarrow K^+\pi^-$, $\bar{D}^0 \rightarrow K^+\pi^-\pi^0$, and $\bar{D}^0 \rightarrow K^+\pi^-\pi^+\pi^-$, we report a joint amplitude analysis of $D^0 \rightarrow \pi^+\pi^-\pi^+\pi^-$ and $D^0 \rightarrow \pi^+\pi^-\pi^0\pi^0(\text{non-}\eta)$. Furthermore, we determine the model-dependent CP -even, absolute branching, and individual component fractions. Throughout this study, the charge-conjugated processes are always implied.

II. BESIII DETECTOR AND MONTE CARLO SIMULATION

The BESIII detector [16] records symmetric e^+e^- collisions provided by the BEPCII storage ring [17] in the center-of-mass energy range from 2.0 to 4.95 GeV, with a peak luminosity of $1 \times 10^{33} \text{ cm}^{-2}\text{s}^{-1}$ achieved at $\sqrt{s} = 3.77 \text{ GeV}$. BESIII has collected large data samples in this energy region [18]. The cylindrical core of the BESIII detector covers 93% of the full solid angle. It comprises a helium-based multilayer drift chamber (MDC), a plastic scintillator time-of-flight system (TOF), and a CsI(Tl) electromagnetic calorimeter (EMC), all enclosed in a superconducting solenoidal magnet providing a 1.0 T magnetic field. The solenoid is supported by an octagonal flux-return yoke with resistive plate counter muon identification modules interleaved with steel. The charged-particle momentum resolution at $1 \text{ GeV}/c$ is 0.5%, and the dE/dx resolution is 6% for resulting Bhabha scatter-

ing electrons. The EMC measures photon energies with a resolution of 2.5% (5%) at 1 GeV in the barrel (end cap) region. The time resolution in the TOF barrel region is 68 ps, while that in the end cap region is 110 ps.

Simulated data samples produced with a geant4-based [19] Monte Carlo (MC) package, which includes the geometric description [20] of the BESIII detector and the detector response, are used to determine detection efficiencies and estimate backgrounds. The simulation models the beam energy spread and initial state radiation (ISR) in the e^+e^- annihilations with the generator kkmc [21, 22]. The inclusive MC sample including the production of $D\bar{D}$ pairs (including quantum coherence for the neutral D channels), the non- $D\bar{D}$ decays of the $\psi(3770)$, the ISR production of the J/ψ and $\psi(3686)$ states, and the continuum processes incorporated in kkmc are generated to estimate the background and ST efficiencies. All particle decays are modeled with evtgen [23, 24] using branching fractions either taken from the Particle Data Group (PDG) [25], when available, or otherwise estimated with lundcharm [26, 27]. Final state radiation from charged final state particles is incorporated using the photos package [28]. Signal MC samples of $D^0 \rightarrow \pi^+\pi^-\pi^+\pi^-$ and $D^0 \rightarrow \pi^+\pi^-\pi^0\pi^0$ generated uniformly in PHSP are used to normalize probability density functions (PDFs) in the amplitude analysis, while those generated according to the amplitude analysis results are used to estimate the DT efficiencies.

III. EVENT SELECTION

Charged tracks detected in the MDC are required to be within a polar angle (θ) range of $|\cos\theta| < 0.93$, where θ is defined with respect to the z axis, which is the symmetry axis of the MDC. The distance of the closest approach of these charged tracks to the interaction point must be less than 10 cm along the z axis and less than 1 cm in the transverse plane. Particle identification (PID) for charged tracks combines measurements of the specific ionization energy loss in the MDC (dE/dx) and the flight time in the TOF to form likelihoods $\mathcal{L}(h)$ ($h = K, \pi$) for each hadron h hypothesis. The charged kaons and pions are identified by comparing the likelihoods for the kaon and pion hypotheses, $\mathcal{L}(K) > \mathcal{L}(\pi)$ and $\mathcal{L}(\pi) > \mathcal{L}(K)$, respectively.

Photon candidates are identified using showers in the EMC. The deposited energy of each shower must be $> 25 \text{ MeV}$ in the barrel region ($|\cos\theta| < 0.80$) and $> 50 \text{ MeV}$ in the end cap region ($0.86 < |\cos\theta| < 0.92$). To exclude showers originating from charged tracks, the angle subtended by the EMC shower and the position of the closest charged track at the EMC must be $> 10^\circ$, as measured from the interaction point. To suppress electronic noises and reject showers unrelated to the event, the difference between the EMC time and the event start time must be

within [0, 700] ns. The π^0 candidates are reconstructed from pairs of photon candidates with the invariant mass being in the interval (0.115, 0.150) GeV/c^2 . To improve the momentum resolution, a kinematic fit constraining the two-photon invariant mass to the known π^0 mass [25] is performed, and the four-momenta updated by this kinematic fit are used in the subsequent analysis.

The signal candidates of $D^0 \rightarrow \pi^+\pi^-\pi^+\pi^-$ and $D^0 \rightarrow \pi^+\pi^-\pi^0\pi^0$ are selected with the DT method [14, 15]. First, the ST \bar{D}^0 mesons are reconstructed with the three hadronic decay modes $\bar{D}^0 \rightarrow K^+\pi^-$, $\bar{D}^0 \rightarrow K^+\pi^-\pi^0$, and $\bar{D}^0 \rightarrow K^+\pi^-\pi^+\pi^-$. Two kinematic variables, the energy difference with respect to the beam energy ΔE and the beam energy constrained mass M_{bc} , are defined as

$$\Delta E = E_{\bar{D}^0} - E_{\text{beam}}, \quad (1)$$

$$M_{bc} = \sqrt{E_{\text{beam}}^2 - \vec{p}_{\bar{D}^0}^2}, \quad (2)$$

where E_{beam} is the beam energy and $E_{\bar{D}^0}$ and $\vec{p}_{\bar{D}^0}$ are the energy and momentum of the ST \bar{D}^0 candidate in the e^+e^- center-of-mass frame. For multiple \bar{D}^0 candidates in each ST mode, only the one with the smallest $|\Delta E|$ is kept for further analysis. To reject the backgrounds from cosmic rays and Bhabha events in the ST mode $\bar{D}^0 \rightarrow K^+\pi^-$, the requirements described in Ref. [29] are applied. To reject the peaking background from the decay $\bar{D}^0 \rightarrow K^+K_S^0\pi^-$ in the ST mode $\bar{D}^0 \rightarrow K^+\pi^-\pi^+\pi^-$, the events with $|M(\pi^+\pi^-) - 0.4976| < 0.03 \text{ GeV}/c^2$ are vetoed. To further reject combinatorial backgrounds, the \bar{D}^0 candidates are required to have ΔE within a given interval defined in Table 1, approximately three times the resolution for each ST mode. In the sub-sample containing ST candidates, the signal candidates of $D^0 \rightarrow \pi^+\pi^-\pi^+\pi^-$ and $D^0 \rightarrow \pi^+\pi^-\pi^0\pi^0$ are reconstructed with the π^\pm and π^0 candidates, which have not been used in the ST side (namely DT thereafter). Similar kinematic variables ΔE and M_{bc} are formed for signal D^0 candidates, and the corresponding ΔE requirements are listed in Table 1. For multiple signal D^0 candidates, only the one giving the smallest $|\Delta E|$ is kept.

To improve the purity of signal candidates in the amplitude analysis, some further selection criteria are applied. The studies based on the inclusive MC sample in-

dicate that most backgrounds from the continuum process $e^+e^- \rightarrow q\bar{q}$ include a K_S^0 in the final state. Therefore, common and secondary vertex fits are performed on all $\pi^+\pi^-$ pairs in the event to reconstruct the K_S^0 candidate. The candidate events are rejected if any K_S^0 candidate with $\pi^+\pi^-$ invariant mass exists within the interval $|M(\pi^+\pi^-) - 0.4976| < 0.03 \text{ GeV}/c^2$ with a decay length greater than twice its resolution. The MC studies also show that most backgrounds from $e^+e^- \rightarrow D^+D^-$ contain decay $D^- \rightarrow K^+\pi^-\pi^-$ owing to its large branching fraction and a similar topology as the signal. The candidate events are rejected if any $K^+\pi^-\pi^-$ combinations exist with $1.863 < M_{bc}(K^+\pi^-\pi^-) < 1.878 \text{ GeV}/c^2$ and $|\Delta E(K^+\pi^-\pi^-)| < 0.03 \text{ GeV}$. The background from the process $e^+e^- \rightarrow D^0\bar{D}^0$ is also considered. Events with any $\pi^+\pi^-\pi^0$ combinations satisfying $1.859 < M_{bc}(\pi^+\pi^-\pi^0) < 1.873 \text{ GeV}/c^2$ and $-0.057 < \Delta E(\pi^+\pi^-\pi^0) < 0.043 \text{ GeV}$ are rejected to eliminate the background of the decay $D^0 \rightarrow \pi^+\pi^-\pi^0$ in the signal process $D^0 \rightarrow \pi^+\pi^-\pi^0\pi^0$. All the above backgrounds do not form peaks in the M_{bc} distribution of the signal side. Additionally, some backgrounds have the same final states as those in the signal mode and produce peaks in the M_{bc} distributions of both the ST and signal sides. To reject the peaking backgrounds from the decays $D^0 \rightarrow K_S^0(\rightarrow \pi^+\pi^-)\pi^+\pi^-$ and $D^0 \rightarrow K^-(\rightarrow \pi^+\pi^-\pi^-)\pi^+$ in the signal process $D^0 \rightarrow \pi^+\pi^-\pi^+\pi^-$, events with $|M(\pi^+\pi^-) - 0.4976| < 0.03 \text{ GeV}/c^2$ or $M(\pi^+\pi^-) < 0.51 \text{ GeV}/c^2$ are vetoed. To reject the peaking backgrounds from the decays $D^0 \rightarrow K_S^0(\rightarrow \pi^0\pi^0)\pi^+\pi^-$, $D^0 \rightarrow K_S^0(\rightarrow \pi^+\pi^-)\pi^0\pi^0$ and $D^0 \rightarrow K^-(\rightarrow \pi^-\pi^0)\pi^+\pi^0$ in the signal process $D^0 \rightarrow \pi^+\pi^-\pi^0\pi^0$, events with $0.4376 < M(\pi^0\pi^0) < 0.5276 \text{ GeV}/c^2$ or $|M(\pi^+\pi^-) - 0.4976| < 0.03 \text{ GeV}/c^2$ or $0.4677 < M(\pi^-\pi^0) < 0.5067 \text{ GeV}/c^2$ are vetoed. Since the interference between the decays $D^0 \rightarrow \pi^0\eta(\rightarrow \pi^+\pi^-\pi^0)$ and $D^0 \rightarrow \pi^+\pi^-\pi^0\pi^0$ is negligible, events with $M(\pi^+\pi^-\pi^0) < 0.57 \text{ GeV}/c^2$ are also vetoed in the signal process $D^0 \rightarrow \pi^+\pi^-\pi^0\pi^0$. Moreover, we reject events if the photon energy from π^0 decays is below 50 MeV, as this indicates an incorrect choice of a soft photon.

IV. BACKGROUND STUDY AND SIGNAL EXTRACTION

Based on the above selection criteria, the two-dimensional (2D) distributions of M_{bc}^{sig} versus M_{bc}^{tag} of the survived events are shown in the left columns of Figs. 2 and 3, where M_{bc}^{sig} and M_{bc}^{tag} are for the signal and tag sides, respectively. Typically, the signal events are accumulated around the intersection of M_{bc}^{sig} and M_{bc}^{tag} at the D^0 nominal mass. The background, arising from miscombinations in the signal and tag sides (namely BKGI thereafter), is located at the diagonal band. Additionally, the backgrounds from $e^+e^- \rightarrow D^0\bar{D}^0$ but with the wrong reconstruction of the signal side exist (namely BKGII) or tag

Table 1. The ΔE requirements for different decay modes.

Decay mode	$\Delta E / \text{GeV}$
$\bar{D}^0 \rightarrow K^+\pi^-$	(-0.027, 0.026)
$\bar{D}^0 \rightarrow K^+\pi^-\pi^0$	(-0.057, 0.043)
$\bar{D}^0 \rightarrow K^+\pi^-\pi^+\pi^-$	(-0.020, 0.018)
$D^0 \rightarrow \pi^+\pi^-\pi^+\pi^-$	(-0.032, 0.028)
$D^0 \rightarrow \pi^+\pi^-\pi^0\pi^0$	(-0.066, 0.041)

side (namely BKGIII), distributed as the vertical and horizontal bands, respectively. Detailed MC studies indicate that most of the backgrounds from $e^+e^- \rightarrow D^0\bar{D}^0$ do not form individual peaks in the distribution of M_{bc}^{sig} or M_{bc}^{tag} . However, backgrounds from $e^+e^- \rightarrow D^0\bar{D}^0$ with $\bar{D}^0 \rightarrow K^+\pi^-\pi^0$ (namely BKGIV) or $D^0 \rightarrow \pi^+\pi^-\pi^0\pi^0$ (namely BKGV) with the wrong reconstruction of π^0 exist, which are exactly consistent with the signal but with the wrong reconstruction of π^0 and produce a relatively broad peak in the M_{bc}^{tag} or M_{bc}^{sig} distribution, respectively. TBackgrounds from the decays $D^0 \rightarrow K_S^0\pi^+\pi^-$, $D^0 \rightarrow K_S^0\pi^0\pi^0$, $D^0 \rightarrow K^-\pi^+\pi^0$, and $D^0 \rightarrow K_S^0\eta'$ (namely BKGVI), which have analogous final states as the signal with the specific decay modes of $K_S^0 \rightarrow \pi^+\pi^-$, $K_S^0 \rightarrow \pi^0\pi^0$, $K^- \rightarrow \pi^-\pi^0$, and $\eta' \rightarrow \gamma\pi^+\pi^-$. These backgrounds are not directly distinguished from the signal in the M_{bc}^{sig} and M_{bc}^{tag} distributions and are estimated by MC simulation. The corresponding yields are summarized in [Table 2](#).

To extract the ST and DT yields, unbinned maximum likelihood fits are performed on the M_{bc}^{tag} distribution of the remaining ST candidates and the 2D distributions of M_{bc}^{sig} versus M_{bc}^{tag} of the remaining DT events in individual tag modes. In the fit to the M_{bc}^{tag} distribution, the signal shape is described by the MC simulated shape of the truth-matched ST events, and the background shape is described by an ARGUS function with the cut-off parameter fixed at 1.8865 GeV/ c^2 [30]. For the $\bar{D}^0 \rightarrow K^+\pi^-\pi^0$ tag mode, an additional peaking background is considered, representing the wrong reconstruction of π^0 , as discussed

above. This peaking background shape is described by the MC-simulated shape of the truth-matched ST events convolved with a bifurcated Gaussian function with fixed parameters obtained from the fit to the corresponding simulated background events. The results of the fits to the M_{bc}^{tag} distributions are shown in [Fig. 1](#).

In the fit to the 2D distribution of M_{bc}^{sig} (labelled as y_1) versus M_{bc}^{tag} (labelled as y_2), the signal is described by

$$S(y_1, y_2) \otimes G(y_1; \mu_{y_1}, \sigma_{y_1}) \otimes G(y_2; \mu_{y_2}, \sigma_{y_2}),$$

where $S(y_1, y_2)$ is the signal MC shape derived from the truth-matched events by using a smoothed 2D histogram, and $G(\mu, \sigma)$ is the Gaussian function describing the resolution difference between data and MC simulation by fixing the parameters $\mu_{y_{1(2)}}$ and $\sigma_{y_{1(2)}}$ to those from the fits on the one-dimensional M_{bc} distributions.

The BKGI is described by

$$T(y_1 - y_2; \mu, \sigma(y_1 + y_2), n) \times A(y_1; m_{y_1}, z'_{y_1}, \rho'_{y_1}) \\ \times A(y_2; m_{y_2}, z'_{y_2}, \rho'_{y_2}),$$

where T is the student's function defined as $T(y; \mu, \sigma, n) = \frac{\Gamma(n/2 + 0.5)}{\sigma \sqrt{n\pi}\Gamma(n/2)} \left[1 + \frac{1}{n} \left(\frac{y - \mu}{\sigma} \right)^2 \right]^{-\frac{n+1}{2}}$, $\sigma(y_1 + y_2) = \sigma_0 + \sigma_1(y_1 + y_2 - m_{y_1} - m_{y_2})$ and A is the ARGUS function defined as

Table 2. The estimated numbers of peaking background events. The uncertainties include the statistical uncertainties of the estimated background yields and the uncertainties of the quoted branching fractions of different background processes.

Signal mode	$\pi^+\pi^-\pi^+\pi^-$			$\pi^+\pi^-\pi^0\pi^0$		
	Tag mode	$K^+\pi^-$	$K^+\pi^-\pi^0$	$K^+\pi^-\pi^+\pi^-$	$K^+\pi^-$	$K^+\pi^-\pi^0$
$N(K_S^0\pi^+\pi^-)$	24.7 ± 2.3	42.4 ± 4.3	22.9 ± 2.6	12.6 ± 3.1	27.7 ± 6.2	29.2 ± 6.2
$N(K_S^0\pi^0\pi^0)$	—	—	—	1.7 ± 0.4	4.3 ± 0.9	2.4 ± 0.6
$N(K^-\pi^+\pi^0)$	—	—	—	12.6 ± 1.2	23.1 ± 2.2	24.0 ± 1.8
$N(K_S^0\eta')$	—	—	—	3.0 ± 1.2	3.9 ± 1.7	2.8 ± 1.2

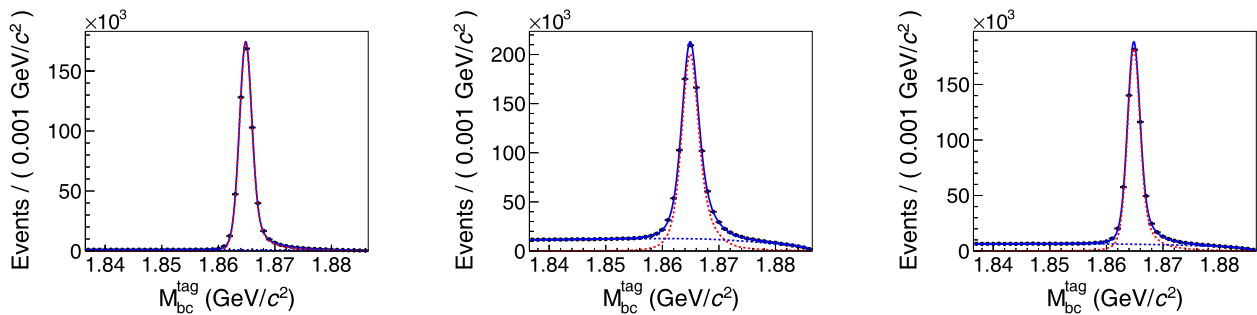


Fig. 1. (color online) The M_{bc}^{tag} distributions of the ST candidates for $\bar{D}^0 \rightarrow K^+\pi^-$ (left), $\bar{D}^0 \rightarrow K^+\pi^-\pi^0$ (middle) and $\bar{D}^0 \rightarrow K^+\pi^-\pi^+\pi^-$ (right). The dots with error bars are the data, the blue solid curves are the total fit results, and the red and blue dashed curves are the signal and background, respectively.

$A(y; m, z, \rho) = y \left(1 - \frac{y^2}{m^2}\right)^\rho e^{z(1 - \frac{y^2}{m^2})}$. In the fit, only the cut-off parameter $m_{y_{1(2)}}$ is fixed to $1.8865 \text{ GeV}/c^2$, the other parameters are free to vary.

The BKGII and BKGIII are described by

$$[S(y_{2(1)}) \otimes G(y_{2(1)}; \mu_{y_{2(1)}}, \sigma_{y_{2(1)}})] \\ \times A(y_{1(2)}; m_{y_{1(2)}}, z_{y_{1(2)}}, \rho_{y_{1(2)}}),$$

where A is the ARGUS function as described above, $S(y_{2(1)})$ is the projection of $S(y_1, y_2)$ on $y_{2(1)}$, and G is the same Gaussian function, as described above. In the fit, the parameter $m_{y_{1(2)}}$ is fixed to $1.8865 \text{ GeV}/c^2$, $\rho_{y_{1(2)}}$ is fixed to the values obtained from the fits to the inclusive MC sample, and $z_{y_{1(2)}}$ is a free parameter.

The BKGIV is described by

$$B_1(y_1, y_2) \otimes G(y_1; \mu_{y_1}, \sigma_{y_1}) \otimes G(y_2; \mu_{y_2}, \sigma_{y_2}),$$

where $B_1(y_1, y_2)$ is the truth-matched signal MC shape $S(y_1, y_2)$ convolved with a bifurcated Gaussian function in y_2 and G is the same Gaussian function, as described above. In the fit, the parameters of the bifurcated Gaussian function are fixed to the values obtained from the fit to the M_{bc}^{tag} distribution of the corresponding simulated background events.

The BKGV in $D^0 \rightarrow \pi^+ \pi^- \pi^0 \pi^0$ is described by

$$B_2(y_1, y_2) \otimes G(y_1; \mu_{y_1}, \sigma_{y_1}) \otimes G(y_2; \mu_{y_2}, \sigma_{y_2}),$$

where $B_2(y_1, y_2)$ is the truth-matched signal MC shape $S(y_1, y_2)$ convolved with a bifurcated Gaussian function in y_1 and G is the same Gaussian function, as described above. In the fit, the parameters of the bifurcated Gaussian function are fixed to the values obtained from the fit to the M_{bc}^{sig} distribution of the corresponding simulated background events.

The BKGVI is described by

$$B_3(y_1, y_2) \otimes G(y_1; \mu_{y_1}, \sigma_{y_1}) \otimes G(y_2; \mu_{y_2}, \sigma_{y_2}),$$

where $B_3(y_1, y_2)$ is the truth-matched MC shape $S(y_1, y_2)$ convolved with a bifurcated Gaussian function in y_1 and G are the Gaussian functions. In the fit, the parameters of the bifurcated Gaussian functions are fixed to the value obtained from the fit to the M_{bc}^{sig} distribution of the corresponding simulated background events from the inclusive MC sample, and the yields are fixed to those summarized in Table 2.

The projections of the 2D fits on M_{bc}^{tag} and M_{bc}^{sig} are shown in Figs. 2 and 3, respectively. The obtained ST and DT yields are summarized in Table 3.

V. AMPLITUDE FORMULA

To improve the resolutions of kinematic variables, a one-constraint kinematic fit with the hypothesis of $D^0 \rightarrow 4\pi$ by constraining the 4π invariant mass to the known D^0 mass [25] is performed on the candidate events, and the updated kinematic variables are used in the amplitude analysis. Using the GPUPWA framework [33], a joint amplitude analysis is performed on the candidate events of $D^0 \rightarrow \pi^+ \pi^- \pi^+ \pi^-$ and $D^0 \rightarrow \pi^+ \pi^- \pi^0 \pi^0$ (non- η). The general amplitude of the $D^0 \rightarrow f$ decay is given by

$$A_f(p) = \sum_i \Lambda_i U_i(p), \quad (3)$$

where U_i is the amplitude of the i -th intermediate process with a complex coupling factor Λ_i and p is a set of four-momenta of final states. For the \bar{D}^0 decay amplitude, assuming CP conservation, the CP -conjugate PHSP \bar{p} is defined by interchanging the charge of the final state and the three-momenta reversal. Then, the amplitude of the $\bar{D}^0 \rightarrow \bar{f}$ decay is given as

$$\bar{A}_{\bar{f}}(p) = \sum_i \Lambda_i \bar{U}_i(p) = \sum_i \Lambda_i U_i(\bar{p}). \quad (4)$$

Since the $D^0 \bar{D}^0$ pair is produced in the $\psi(3770)$ decay, quantum correlation between D^0 and \bar{D}^0 needs to be considered. By ignoring the effects of CP violation and D^0 - \bar{D}^0 mixing, the observed differential cross section $|M_f(p)|^2$ of $D^0 \rightarrow f$ and the tag mode $\bar{D}^0 \rightarrow \bar{g}$ is

$$|A_f(p) - r_g R_g e^{-i\delta_g} \bar{A}_{\bar{f}}(p)|^2 + r_g^2 (1 - R_g^2) |\bar{A}_f(p)|^2, \quad (5)$$

$$\text{where } r_g^2 = \frac{\int |\bar{A}_g|^2 d\Phi_g}{\int |A_g|^2 d\Phi_g}, \quad R_g e^{-i\delta_g} = \frac{\int A_g^* \bar{A}_g d\Phi_g}{\sqrt{\int |A_g|^2 d\Phi_g \int |\bar{A}_g|^2 d\Phi_g}}.$$

The values of r , R , and δ for the three tag modes are summarized in Table 4. The second term in Eq. (5) is ignored in practice owing to the relatively small value of $r_g^2 (1 - R_g^2)$.

The amplitude U_i is constructed with the spin factor, Blatt-Weisskopf barrier factors [34], and resonance propagators. To construct U_i of the four-body D^0 decay, the isobar model is applied, factorizing the decay into subsequent two-body decay amplitudes [35–37]. The general amplitude of the i -th intermediate process in a four-body decay is given by

$$U_i(p) = S_i(p) B_{L_D}(p) P_{R_1}(p) B_{L_{R_1}}(p) P_{R_2}(p) B_{L_{R_2}}(p), \quad (6)$$

where S_i is the spin factor of the i -th decay amplitude,

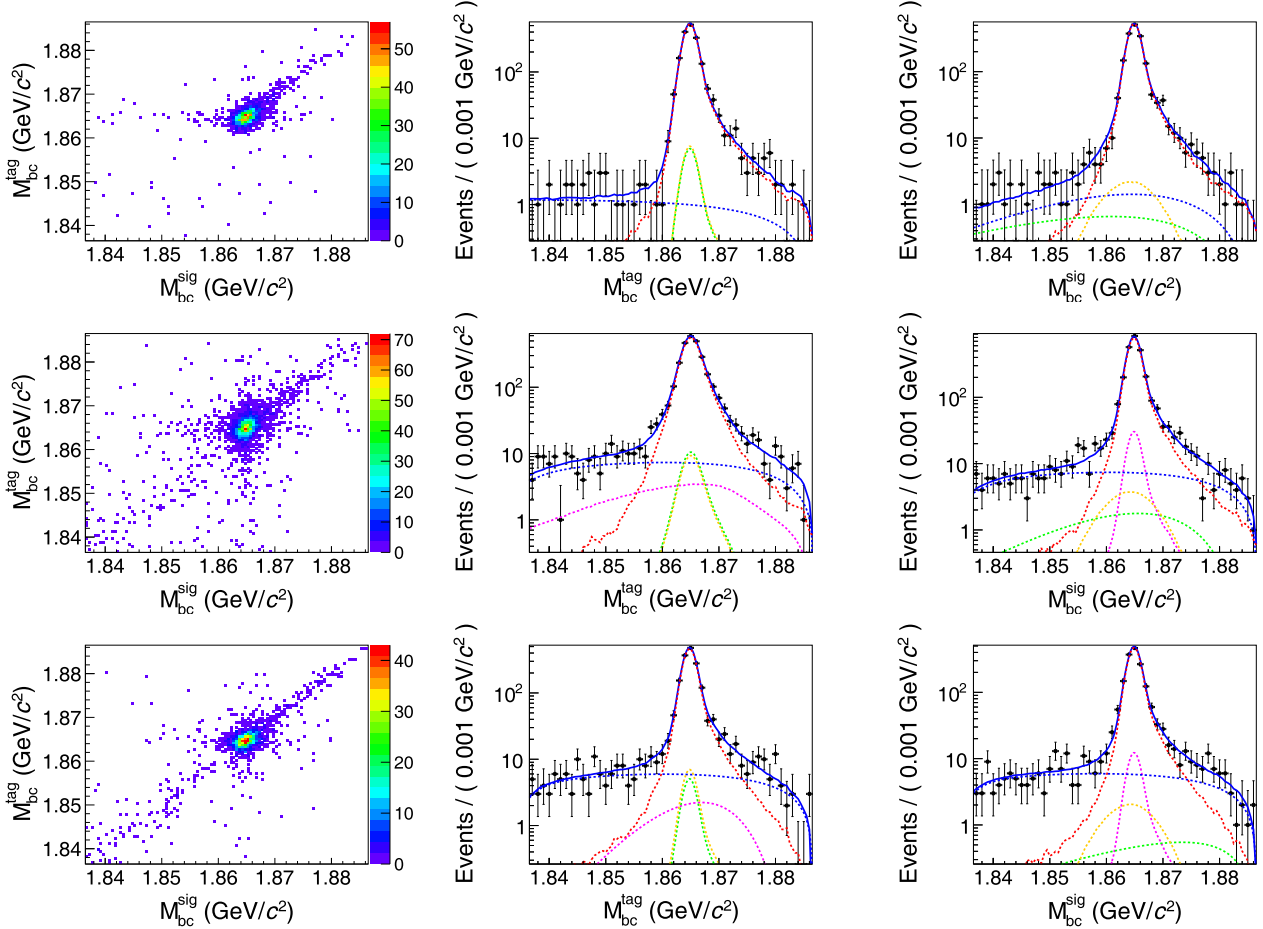


Fig. 2. (color online) The 2D distributions (left) of M_{bc}^{tag} versus M_{bc}^{sig} and the projections on M_{bc}^{tag} (middle) and M_{bc}^{sig} (right) of the 2D fits on the DT events tagged by $\bar{D}^0 \rightarrow K^+ \pi^-$ (first row), $\bar{D}^0 \rightarrow K^+ \pi^- \pi^0$ (second row), and $\bar{D}^0 \rightarrow K^+ \pi^- \pi^+ \pi^-$ (third row) in the $D^0 \rightarrow \pi^+ \pi^- \pi^+ \pi^-$ decay. The dots with error bars are the data. The blue solid curves are the total fit results, and the red dashed curves show the signal. The green, blue, orange, and magenta dashed curves are BKGI, BKGIII, BKGVI, and the combination of BKGII and BKGV, respectively.

B_{L_X} ($X = D, R_1, R_2$) are the Blatt-Weisskopf barrier factors for the D meson and the resonances R_1 and R_2 , and P_{R_1} and P_{R_2} are the propagators of R_1 and R_2 , respectively. The amplitude is constructed with the exchange symmetry for indistinguishable pions.

The spin factor is constructed with the covariant Zemach (Rarita-Schwinger) tensor formalism [38–41] by combining pure-orbital-angular-momentum covariant tensors $\tilde{r}_{\mu_1 \dots \mu_L}^{(L)}$ and the momenta of parent particles together with Minkowski metric $g_{\mu\nu}$ and Levi-Civita symbol $\epsilon_{\mu\nu\lambda\sigma}$. For a process $a \rightarrow bc$, the covariant tensors $\tilde{r}_{\mu_1 \dots \mu_L}^{(L)}$ for the final states of pure orbital angular momentum L are

$$\tilde{r}_{\mu_1 \dots \mu_L}^{(L)} = (-1)^L P_{\mu_1 \dots \mu_L \mu'_1 \dots \mu'_L}^{(L)}(p_a) r^{\mu'_1} \dots r^{\mu'_L}, \quad (7)$$

where $r = p_b - p_c$ and $P_{\mu_1 \dots \mu_L \mu'_1 \dots \mu'_L}^{(L)}(p_a)$ is the spin projection operator of the particle a ,

$$P^{(0)}(p_a) = 1, \quad (8)$$

$$P_{\mu\mu'}^{(1)}(p_a) = -g_{\mu\mu'} + \frac{P_{a\mu}P_{a\mu'}}{p_a^2}, \quad (9)$$

$$P_{\mu\mu'\nu'}^{(2)}(p_a) = \frac{1}{2} [P_{\mu\mu'}^{(1)}(p_a) P_{\nu\nu'}^{(1)}(p_a) + P_{\mu\nu'}^{(1)}(p_a) P_{\nu\mu'}^{(1)}(p_a)] - \frac{1}{3} P_{\mu\nu}^{(1)}(p_a) P_{\mu'\nu'}^{(1)}(p_a). \quad (10)$$

Following the isobar model, the spin factors of the four-body decay $D^0 \rightarrow P_1 P_2 P_3 P_4$ are summarized in Table 5.

The Blatt-Weisskopf barrier factors $B_L(q)$ are derived by assuming a square well interaction potential as

$$B_{L=0}(q) = 1, \quad (11)$$

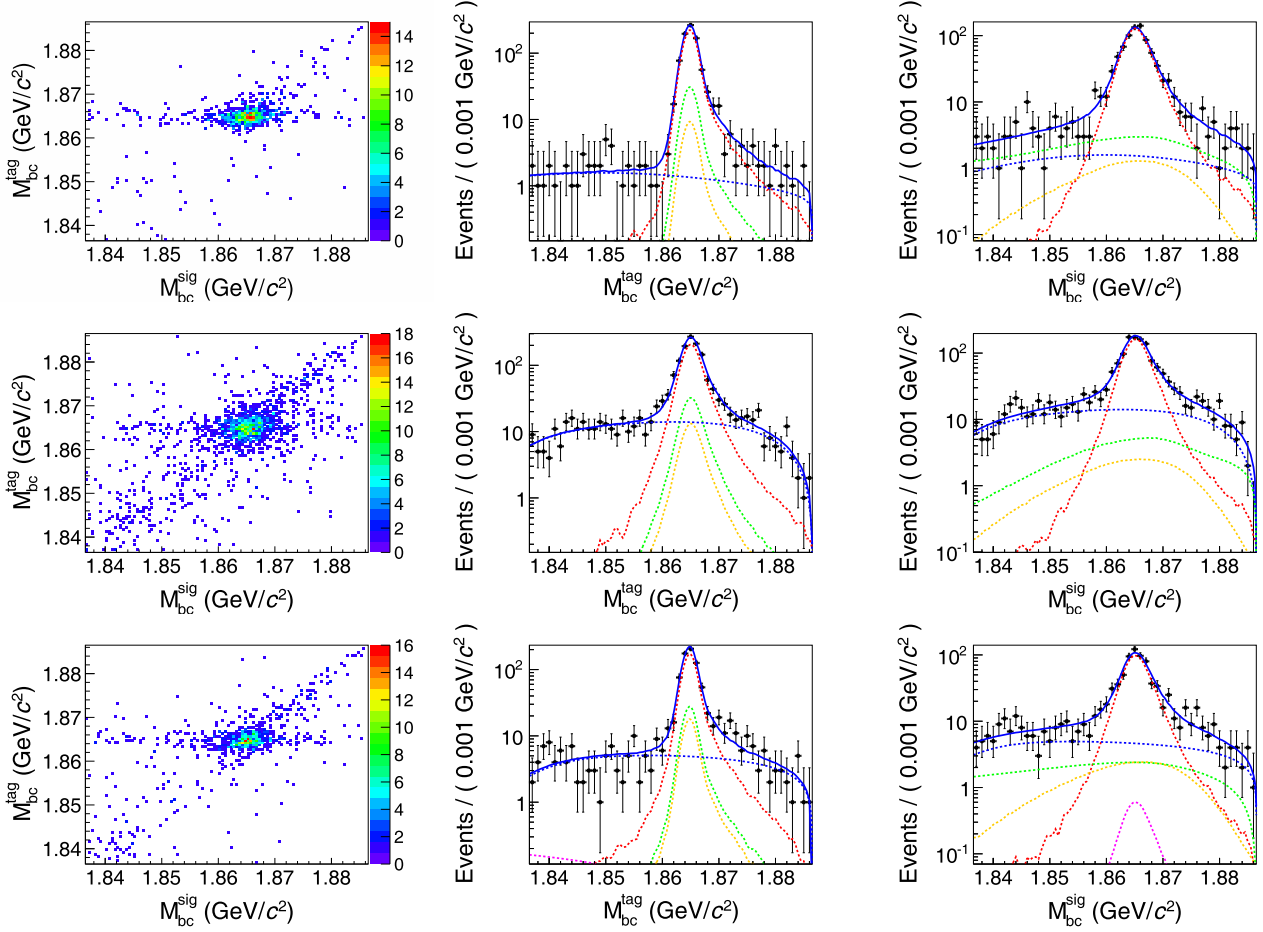


Fig. 3. (color online) The 2D distributions (left) of M_{bc}^{tag} versus M_{bc}^{sig} and the projections on M_{bc}^{tag} (middle) and M_{bc}^{sig} (right) of the 2D fits on the DT events tagged by $\bar{D}^0 \rightarrow K^+\pi^-$ (first row), $\bar{D}^0 \rightarrow K^+\pi^-\pi^0$ (second row) and $\bar{D}^0 \rightarrow K^+\pi^-\pi^+\pi^-$ (third row) in the $D^0 \rightarrow \pi^+\pi^-\pi^0\pi^0$ decay. The dots with error bars are the data. The blue solid curves are the total fit results, and the red dashed curves show the signal. The green dashed curves are the combination of BKGII and BKGIV, the magenta dashed curves are the combination of BKGII and BKGVI, the blue and orange dashed curves are BKGIII and BKGVI, respectively.

Table 3. The ST and DT yields, efficiencies, and quantum correlated correction factors for three tag modes.

Tag mode	$\bar{D}^0 \rightarrow K^+\pi^-$	$\bar{D}^0 \rightarrow K^+\pi^-\pi^0$	$\bar{D}^0 \rightarrow K^+\pi^-\pi^+\pi^-$
N^{ST}	549586 ± 778	914531 ± 1321	600316 ± 856
ϵ^{ST}	0.6762 ± 0.0004	0.2953 ± 0.0001	0.3365 ± 0.0002
$N_{\pi^+\pi^-\pi^+\pi^-}^{DT}$	1719 ± 42	2560 ± 56	1520 ± 43
$\epsilon_{\pi^+\pi^-\pi^+\pi^-}^{DT}$	0.2792 ± 0.0006	0.1187 ± 0.0002	0.1221 ± 0.0003
$N_{\pi^+\pi^-\pi^0\pi^0}^{DT}$ (non- η)	721 ± 32	917 ± 39	562 ± 29
$\epsilon_{\pi^+\pi^-\pi^0\pi^0}^{DT}$ (non- η)	0.0818 ± 0.0003	0.0319 ± 0.0001	0.0334 ± 0.0001
$\frac{2rR\cos\delta}{1+r^2}$	-0.114 ± 0.004 [31]	-0.067 ± 0.005 [32]	$-0.046^{+0.013}_{-0.011}$ [32]

Table 4. The input values of r , R , and δ for the three tag modes.

Mode	$K^-\pi^+$	$K^-\pi^+\pi^0$	$K^-\pi^+\pi^-\pi^+$
$r(\%)$	5.86 ± 0.02 [31]	4.41 ± 0.11 [32]	5.50 ± 0.07 [32]
R	1	0.79 ± 0.04 [32]	$0.44^{+0.09}_{-0.10}$ [32]
$\delta(^{\circ})$	$192.1^{+8.6}_{-10.2}$ [31]	196 ± 11 [32]	161^{+28}_{-18} [32]

Table 5. Summary of the spin factors in this analysis, where S , P , V , A , T , and PT denote scalar, pseudo-scalar, vector, axial-vector, tensor, and pseudo-tensor mesons, respectively. $[S]$, $[P]$, and $[D]$ represent orbital angular momenta $L = 0, 1$, and 2 in the decays, respectively.

Decay chain	Spin factor
$D[S] \rightarrow PP_1, P[S] \rightarrow SP_2, S[S] \rightarrow P_3P_4$	1
$D[S] \rightarrow PP_1, P[P] \rightarrow VP_2, V[P] \rightarrow P_3P_4$	$\tilde{t}_\mu(P)\tilde{t}^\mu(V)$
$D[S] \rightarrow PP_1, P[D] \rightarrow TP_2, T[D] \rightarrow P_3P_4$	$\tilde{t}_{\mu\nu}(P)\tilde{t}^{\mu\nu}(T)$
$D[P] \rightarrow AP_1, A[S] \rightarrow VP_2, V[P] \rightarrow P_3P_4$	$\tilde{t}_\mu(D)P^{\mu\nu}(A)\tilde{t}_\nu(V)$
$D[P] \rightarrow AP_1, A[D] \rightarrow VP_2, V[P] \rightarrow P_3P_4$	$\tilde{t}_\mu(D)\tilde{t}^{\mu\nu}(A)\tilde{t}_\nu(V)$
$D[P] \rightarrow AP_1, A[P] \rightarrow SP_2, S[S] \rightarrow P_3P_4$	$\tilde{t}_\mu(D)\tilde{t}^\mu(A)$
$D[P] \rightarrow AP_1, A[P] \rightarrow TP_2, T[D] \rightarrow P_3P_4$	$\tilde{t}_\mu(D)\tilde{t}_\nu(A)P^{\mu\nu\rho\sigma}(A)\tilde{t}_{\rho\sigma}(T)$
$D[P] \rightarrow V_1P_1, V_1[P] \rightarrow V_2P_2, V_2[P] \rightarrow P_3P_4$	$\tilde{t}_\mu(D)P^{\mu\nu}(V_1)\epsilon_{\nu\lambda\sigma\rho}p_{V_1}^\rho\tilde{t}^l(V_1)\tilde{t}^\nu(V_2)$
$D[D] \rightarrow PTP_1, PT[S] \rightarrow TP_2, T[D] \rightarrow P_3P_4$	$\tilde{t}_{\mu\nu}(D)P^{\mu\nu\alpha\beta}(PT)\tilde{t}_{\alpha\beta}(T)$
$D[D] \rightarrow PTP_1, PT[P] \rightarrow VP_2, V[P] \rightarrow P_3P_4$	$\tilde{t}_{\mu\nu}(D)P^{\mu\nu\alpha\beta}(PT)\tilde{t}_\alpha(PT)\tilde{t}_\beta(V)$
$D[D] \rightarrow PTP_1, PT[D] \rightarrow SP_2, S[S] \rightarrow P_3P_4$	$\tilde{t}_{\mu\nu}(D)\tilde{t}^{\mu\nu}(PT)$
$D[D] \rightarrow TP_1, T[D] \rightarrow VP_2, V[P] \rightarrow P_3P_4$	$\tilde{t}_{\mu\nu}(D)P^{\mu\nu\alpha\beta}(T)\epsilon_{\alpha\lambda\sigma\rho}p_T^\rho\tilde{t}_\beta^l(T)P^{\sigma\gamma}(T)\tilde{t}_\gamma(V)$
$D[D] \rightarrow T_1P_1, T_1[P] \rightarrow T_2P_2, T_2[D] \rightarrow P_3P_4$	$\tilde{t}_{\mu\nu}(D)P^{\mu\nu\alpha\beta}(T_1)\epsilon_{\alpha\lambda\sigma\rho}p_{T_1}^\rho\tilde{t}^l(T_1)\tilde{t}_\beta^\nu(T_2)$
$D[S] \rightarrow S_1S_2, S_1[S] \rightarrow P_1P_2, S_2[S] \rightarrow P_3P_4$	1
$D[P] \rightarrow VS, V[P] \rightarrow P_1P_2, S[S] \rightarrow P_3P_4$	$\tilde{t}_\mu(D)\tilde{t}^\mu(V)$
$D[S] \rightarrow V_1V_2, V_1[P] \rightarrow P_1P_2, V_2[P] \rightarrow P_3P_4$	$\tilde{t}_\mu(V_1)\tilde{t}^\mu(V_2)$
$D[P] \rightarrow V_1V_2, V_1[P] \rightarrow P_1P_2, V_2[P] \rightarrow P_3P_4$	$\epsilon_{\mu\nu\alpha\beta}p_D^\beta\tilde{t}^\mu(D)\tilde{t}^\nu(V_1)\tilde{t}^\alpha(V_2)$
$D[D] \rightarrow V_1V_2, V_1[P] \rightarrow P_1P_2, V_2[P] \rightarrow P_3P_4$	$\tilde{t}_{\mu\nu}(D)\tilde{t}^\mu(V_1)\tilde{t}^\nu(V_2)$
$D[D] \rightarrow TS, T[D] \rightarrow P_1P_2, S[S] \rightarrow P_3P_4$	$\tilde{t}_{\mu\nu}(D)\tilde{t}^{\mu\nu}(T)$
$D[P] \rightarrow TV, T[D] \rightarrow P_1P_2, V[P] \rightarrow P_3P_4$	$\tilde{t}_\mu(D)\tilde{t}^{\mu\nu}(T)\tilde{t}_\nu(V)$
$D[D] \rightarrow TV, T[D] \rightarrow P_1P_2, V[P] \rightarrow P_3P_4$	$\epsilon_{\mu\nu\alpha\beta}p_D^\beta\tilde{t}^{\mu\rho}(D)\tilde{t}_\rho^\nu(T)\tilde{t}^\alpha(V)$
$D[S] \rightarrow T_1T_2, T_1[D] \rightarrow P_1P_2, T_2[D] \rightarrow P_3P_4$	$\tilde{t}_{\mu\nu}(T_1)\tilde{t}^{\mu\nu}(T_2)$
$D[P] \rightarrow T_1T_2, T_1[D] \rightarrow P_1P_2, T_2[D] \rightarrow P_3P_4$	$\epsilon_{\mu\nu\alpha\beta}p_D^\beta\tilde{t}^\mu(D)\tilde{t}^{\rho\sigma}(T_1)\tilde{t}_\rho^\nu(T_2)$
$D[D] \rightarrow T_1T_2, T_1[D] \rightarrow P_1P_2, T_2[D] \rightarrow P_3P_4$	$\tilde{t}_{\mu\nu}(D)\tilde{t}^{\mu\rho}(T_1)\tilde{t}_\rho^\nu(T_2)$

$$B_{L=1}(q) = \sqrt{\frac{2}{q^2 + q_R^2}}, \quad (12)$$

$$B_{L=2}(q) = \sqrt{\frac{13}{q^4 + 3q^2q_R^2 + 9q_R^4}}, \quad (13)$$

where q is the momentum of the daughter particle in the rest frame of the mother particle, L is the orbital angular momentum, and $q_R = 1/R$ is a hadron "scale" parameter (R denotes the radius of the centrifugal barrier). In this analysis, the radius R is taken to be $5.0 \text{ GeV}^{-1}c$ for D^0 mesons, and $3.0 \text{ GeV}^{-1}c$ for other intermediate resonances.

The resonance propagators are generally described by a relativistic Breit-Wigner function

$$P(s) = \frac{1}{m_0^2 - s - i\sqrt{s}\Gamma(s)}, \quad (14)$$

where m_0 is the nominal mass of the resonance. For a resonance decaying into two scalar particles $a \rightarrow bc$, $\Gamma_{a \rightarrow bc}(s)$ is given by

$$\Gamma_{a \rightarrow bc}(s) = \Gamma_0^{a \rightarrow bc} \left(\frac{q}{q_0}\right)^{2L+1} \left(\frac{m_0}{\sqrt{s}}\right)^2 \left(\frac{B_L(q)}{B_L(q_0)}\right)^2, \quad (15)$$

where $\Gamma_0^{a \rightarrow bc}$ is the nominal width when $s = m_0^2$ and q_0 is the corresponding momentum of the daughter particle in the rest frame of the mother particle.

In this analysis, the propagators of $\rho(770)$ and $\rho(1450)$ are described by the Gounaris-Sakurai parametrization [42]. The propagator of $f_0(980)$ in the decay $a_1(1420) \rightarrow f_0(980)\pi$ is described by a Flatté parametrization of $\pi\pi$ and KK coupled channels with parameters from Ref. [43].

The K -matrix parametrization [44, 45] instead of the Breit-Wigner formula is adopted for the $\pi\pi$ S -wave. The P -vector parametrization of the K -matrix for the $\pi\pi$ S -

wave with five coupled channels $\pi\pi$, KK , $\pi\pi\pi\pi$, $\eta\eta$, $\eta\eta'$ and five poles is written as

$$F_\mu(s) = [I - iK(s)\rho(s)]_{\mu\nu}^{-1} P_\nu(s), \quad (16)$$

where I is the identity matrix, K is the K -matrix describing the scattering process, ρ is the PHSP matrix, and P is the initial production vector (P -vector). The indices μ and ν denote the coupled channels ($\pi\pi$, KK , $\pi\pi\pi\pi$, $\eta\eta$, and $\eta\eta'$), and only $F_\mu(s)$ of the $\pi\pi$ component is used as the propagator of the $\pi\pi$ S-wave. The K -matrix is given by

$$K_{\mu\nu}(s) = \left(\sum_\alpha \frac{g_\mu^\alpha g_\nu^\alpha}{m_\alpha^2 - s} + f_{\mu\nu}^{\text{scatt}} \frac{1 - s_0^{\text{scatt}}}{s - s_0^{\text{scatt}}} \right) f_{A0}(s), \quad (17)$$

containing five poles ($\alpha = 1-5$). The K -matrix parameters are fixed to those in Ref. [45]. The P -vector is written as

$$P_\nu(s) = \left(\sum_\alpha \frac{\beta_\alpha g_\nu^\alpha}{m_\alpha^2 - s} + f_\nu^{\text{prod}} \frac{1 - s_0^{\text{prod}}}{s - s_0^{\text{prod}}} \right), \quad (18)$$

where the poles are the same as those for the K -matrix. The parameters β_α and f_ν^{prod} are free in the fit. For the parameter s_0^{prod} in the P -vector, we assume that they take the same value in all $\pi\pi$ S-waves and fix them to $-5 \text{ GeV}^2/c^4$ since they are insensitive to any choice if $s_0^{\text{prod}} \leq -5 \text{ GeV}^2/c^4$ in our fit.

In practice, two $\pi\pi$ S-waves exist in the decay $D^0 \rightarrow S_1 S_2$, and the corresponding propagator is

$$F'_{\mu\nu}(s_1, s_2) = [I - iK(s_1)\rho(s_1)]_{\mu\rho}^{-1} [I - iK(s_2)\rho(s_2)]_{\rho\nu}^{-1} \times P_{\rho\sigma}(s_1, s_2), \quad (19)$$

where s_1 and s_2 are the invariant masses squared of $\pi\pi$, $P_{\rho\sigma}(s_1, s_2)$ is the expansion of the product of two P -vectors $P_\rho(s_1)$ and $P_\sigma(s_2)$, and the corresponding coefficients of each term are taken to be independent parameters in the fit. Benefiting from the exchange symmetry of two $\pi\pi$ S-waves in the amplitude, $P_{\rho\sigma}(s_1, s_2)$ can be written as

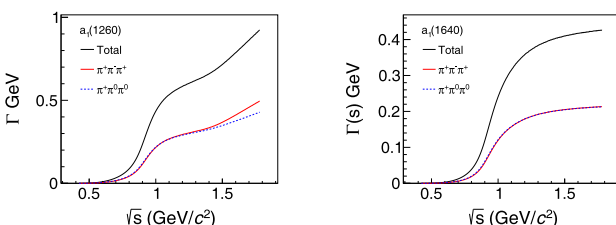


Fig. 4. (color online) The $\Gamma(s)$ of $a_1(1260)$, $a_1(1640)$, $h_1(1170)$, and $\pi(1300)$ resonances obtained in the amplitude analysis.

$$\begin{aligned} P_{\rho\sigma}(s_1, s_2) = & \sum_{\alpha\beta}^{|\alpha|<\beta} a_{\alpha\beta} \left[\frac{g_\rho^\alpha g_\sigma^\beta}{(m_\alpha^2 - s_1)(m_\beta^2 - s_2)} + \frac{g_\rho^\beta g_\sigma^\alpha}{(m_\beta^2 - s_1)(m_\alpha^2 - s_2)} \right] \\ & + \sum_\alpha b_{\alpha,\rho} \frac{g_\sigma^\alpha (1 - s_0^{\text{prod}})}{(s_1 - s_0^{\text{prod}})(m_\alpha^2 - s_2)} \\ & + \sum_\alpha b_{\alpha,\sigma} \frac{g_\rho^\alpha (1 - s_0^{\text{prod}})}{(s_2 - s_0^{\text{prod}})(m_\alpha^2 - s_1)} \\ & + c_{[\rho,\sigma]} \frac{(1 - s_0^{\text{prod}})^2}{(s_1 - s_0^{\text{prod}})(s_2 - s_0^{\text{prod}})}, \end{aligned} \quad (20)$$

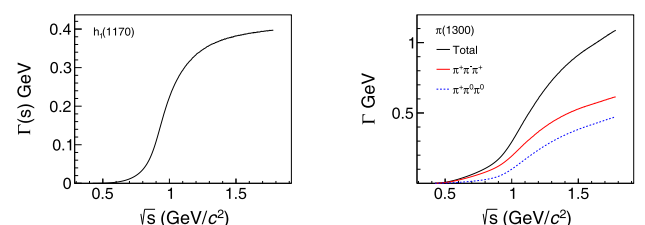
where $c_{[\rho,\sigma]} = c_{\rho,\sigma} + c_{\sigma,\rho}$, and $c_{[\rho,\sigma]}$ with $\rho > \sigma$ is fixed to zero in the fit. Similar to one $\pi\pi$ S-wave, only the $(\pi\pi, \pi\pi)$ component of $F'_{\mu\nu}$ is used.

The propagators of the resonances $a_1(1260)$, $a_1(1640)$, $h_1(1170)$ and $\pi(1300)$ decaying into 3π are described by relativistic Breit-Wigner functions with the coupled channel 3π , where $\Gamma(s)$ are obtained by integrating the amplitude squared over PHSP

$$\Gamma_{a \rightarrow bcd}(s) \propto \frac{m_0}{\sqrt{s}} \int \sum_{\text{spin}} |A_{a \rightarrow bcd}|^2 d\Phi_3, \quad (21)$$

based on the amplitudes $A_{R \rightarrow 3\pi}$ obtained in this analysis. Figure 4 shows the $\Gamma(s)$ obtained in the amplitude analysis. For other resonances decaying into 3π , a relativistic Breit-Wigner function with a constant $\Gamma(s)$ is used. The parameters of $a_1(1260)$ and $\pi(1300)$ are determined in the fit and others are fixed to their respective PDG values [25]. Owing to its small contribution, the $a_1(1420)$ is described as a relativistic Breit-Wigner function with a constant $\Gamma(s)$, even though it has been regarded as the effect of the Triangle Singularity [46]. Only the decay of $a_1(1420) \rightarrow f_0(980)\pi$ is considered, and the corresponding resonant parameters are taken from Ref. [47].

To account for the resolution effect for the narrow resonances $\phi(1020)$ and $\omega(782)$, the shapes of the corresponding relativistic Breit-Wigner functions in the $M(\pi^+\pi^-\pi^0)$ distribution are convolved with a Gaussian function. The parameters of this Gaussian function are obtained by the fit to the η peak in the $M(\pi^+\pi^-\pi^0)$ distribution with the Breit-Wigner function of η convolved with the same Gaussian function.



In this analysis, two decay topologies, $D \rightarrow R_1 R_2$ and $D \rightarrow R_1 \pi \rightarrow R_2 \pi \pi$, are considered. Meanwhile, the isospin symmetry is considered by applying the Clebsch-Gordan (CG) coefficients between the isospin processes. The isospin states for the u and d quarks are

$$|u\rangle : |\frac{1}{2}, \frac{1}{2}\rangle, |\bar{u}\rangle : -|\frac{1}{2}, -\frac{1}{2}\rangle, |d\rangle : |\frac{1}{2}, -\frac{1}{2}\rangle, |\bar{d}\rangle : |\frac{1}{2}, \frac{1}{2}\rangle. \quad (22)$$

Based on the quark components of hadrons, the isospin states of the hadrons are shown in Table 6. The isospin amplitudes for typical processes are written as

$$\begin{aligned} A(D^0 \rightarrow a_1^+ \pi^-) &= A(\rho_{\pi^+ \pi^-}^0, \pi^+) + A(\rho_{\pi^+ \pi^0}^+, \pi^-) \\ &- c[2A(f_{\pi^+ \pi^-} \pi^+, \pi^-) + A(f_{\pi^0 \pi^0} \pi^+, \pi^-)], \end{aligned} \quad (23)$$

$$\begin{aligned} A(D^0 \rightarrow a_1^0 \pi^0) &= -A(\rho_{\pi^+ \pi^0}^+, \pi^0) + A(\rho_{\pi^0 \pi^-}^-, \pi^0) \\ &- c[2A(f_{\pi^+ \pi^-} \pi^0, \pi^0) + A(f_{\pi^0 \pi^0} \pi^0, \pi^0)], \end{aligned} \quad (24)$$

$$\begin{aligned} A(D^0 \rightarrow a_1^- \pi^+) &= -A(\rho_{\pi^+ \pi^-}^0, \pi^+) - A(\rho_{\pi^0 \pi^-}^-, \pi^+) \\ &- c[2A(f_{\pi^+ \pi^-} \pi^-, \pi^+) + A(f_{\pi^0 \pi^0} \pi^-, \pi^+)], \end{aligned} \quad (25)$$

$$\begin{aligned} A(D^0 \rightarrow h_1^0 \pi^0) &= -A(\rho_{\pi^+ \pi^0}^+, \pi^0) - A(\rho_{\pi^0 \pi^-}^-, \pi^0) \\ &+ A(\rho_{\pi^+ \pi^-}^0, \pi^0), \end{aligned} \quad (26)$$

$$\begin{aligned} A(D^0 \rightarrow f f') &= 4A(f_{\pi^+ \pi^-}, f'_{\pi^+ \pi^-}) + 2[A(f_{\pi^+ \pi^-}, f'_{\pi^0 \pi^0}) \\ &+ A(f_{\pi^0 \pi^0}, f'_{\pi^+ \pi^-})] + A(f_{\pi^0 \pi^0}, f'_{\pi^0 \pi^0}), \end{aligned} \quad (27)$$

$$A(D^0 \rightarrow \rho^0 f) = 2A(\rho_{\pi^+ \pi^-}^0, f_{\pi^+ \pi^-}) + A(\rho_{\pi^+ \pi^-}^0, f_{\pi^0 \pi^0}). \quad (28)$$

Here, a_1 and ρ are isospin vectors, whereas h_1 and $f^{(\prime)}$ are isospin scalars. The normalization factors are dropped here and c is the relative difference (including magnitude and phase) between two isospin processes determined in the amplitude analysis.

Table 6. The quark components and isospin states for different hadrons used in the analysis.

	π^+, b^+, ρ^+, a^+	π^0, b^0, ρ^0, a^0	π^-, b^-, ρ^-, a^-
$I = 1$	$ u\bar{d}\rangle : 1, 1\rangle$	$ \frac{u\bar{u} - d\bar{d}}{\sqrt{2}}\rangle : - 1, 0\rangle$ h, ω, ϕ, f	$ d\bar{u}\rangle : - 1, -1\rangle$
$I = 0$		$ (u\bar{u} + d\bar{d}) + g(s\bar{s})\rangle : - 0, 0\rangle$	

VI. AMPLITUDE FIT PROCESS AND RESULT

In the amplitude fit, the sPlot technique [48] is applied to deal with the background effect. In the sPlot method, the four-momenta of the final states are chosen as control variables x , M_{bc}^{sig} and M_{bc}^{tag} are chosen as discriminating variables y , and the weight for each candidate event is obtained by an unbinned maximum likelihood fit on the 2D distribution of M_{bc}^{sig} versus M_{bc}^{tag} , as described in Sec. IV.

According to the sPlot technique and based on the above DT fit, the weight $W_s(y)$ of each candidate event is calculated as

$$W_s(y) = \frac{\sum_i V_{si} F_i(y)}{\sum_i N_j F_j(y) + \sum_k N'_k F'_k(y)}, \quad (29)$$

where the index s denotes the signal, $F_{i(j)}(y)$ are the PDFs of the signal ($i(j) = s$) and backgrounds ($i(j) \neq s$) from BKGI to BGKV with floating yields, $F'_k(y)$ are the PDFs of BKGVI with fixed yields, and $N_{i(j)}$ and N'_k are the corresponding yields for each component. The inverse of covariance matrix V_{ij} is calculated with

$$V_{ij}^{-1} = \sum_{n \in \text{Data}} \frac{F_i(y_n) F_j(y_n)}{(\sum_k N_k F_k(y_n) + \sum_l N'_l F'_l(y_n))^2}, \quad (30)$$

where the summations for indices k and l run over all the components of $F_k(y)$ and $F'_l(y)$, as described above, respectively. The summation for index n runs over all the events in the DT fit.

Based on the sPlot technique, $W_s(y)$, defined in Eq. (29), includes the effects of the backgrounds with a fixed number of events. To account for these effects, the coefficients c_i are calculated as

$$c_i = \sum_j V_{sj} v_{ij}, \quad (31)$$

where the summation runs over the signal and backgrounds from BKGI to BKGVI with floating yields in the fit, i represents the different components in the BKGVI, and v_{ij} is

$$v_{ij} = \sum_{n \in \text{Data}} \frac{F'_i(y_n) F_j(y_n)}{(\sum_k N_k F_k(y_n) + \sum_l N'_l F'_l(y_n))^2}. \quad (32)$$

With the obtained $W_s(y)$ and c_i , the x distribution of all candidate events with the weight $W_s(y)$ is the real signal together with the contributions of the peaking background in BKGVI,

$$N_s P_s(x) + \sum_j c_j N'_j P'_j(x), \quad (33)$$

where $P_s(x)$ and $P'_j(x)$ are the x distributions of the signal and the peaking background j in the BKGVI and N_s and N'_j are the corresponding yields obtained from the above 2D fit and MC simulation, respectively.

In practice, the PDF of observing a signal event with the given final kinematic p is written as

$$P_s(p) = \frac{\epsilon_s(p)|M_f(p)|^2\phi_4(p)}{\int \epsilon_s(p)|M_f(p)|^2 d\Phi_4}, \quad (34)$$

where $\epsilon_s(p)$ is the signal efficiency, $|M_f(p)|^2$ is the differential cross section, as discussed in Sec. V, and $\phi_4(p)$ is the PHSP density. The normalization factor is calculated by MC integration with the PHSP signal MC sample after event selection,

$$\int \epsilon_s(p)|M_f(p)|^2 d\Phi_4 \propto \frac{1}{N_{MC}} \sum_{i=1}^{N_{MC}} |M_f(p_i)|^2. \quad (35)$$

where the N_{MC} is the number of events of the PHSP signal MC. According to Eq. (33), the weighted likelihood $\ln L$ is given by

$$f \left[\sum_{i \in \text{Data}} W_s(y_i) \ln P_s(p_i) - \sum_j \sum_{i \in \text{BMC}_j} \omega_j \ln P_s(p_i) \right], \quad (36)$$

where the second term in the bracket is the contribution from the peaking background, estimated using the corresponding simulated background MC (BMC). The normalization factor ω_j is given by

$$\omega_j = c_j N_{\text{BKG}_j}^{\text{Data}} / N_{\text{BKG}_j}^{\text{MC}}. \quad (37)$$

Here, c_j is obtained from Eq. (31), and $N_{\text{BKG}_j}^{\text{Data}}$ and $N_{\text{BKG}_j}^{\text{MC}}$ are the background yields in the data and simulated background events, respectively. The factor f in Eq. (36),

$$f = \frac{\sum_{i \in \text{Data}} W_s(y_i) + \sum_j \omega_j N_{\text{BKG}_j}^{\text{MC}}}{\sum_{i \in \text{Data}} W_s^2(y_i) + \sum_j \omega_j^2 N_{\text{BKG}_j}^{\text{MC}}}, \quad (38)$$

is the global factor to correct the statistical bias in the weighted maximum likelihood fit.

The total likelihood function in this analysis is summed over the two signal channels and three tag modes,

$$\ln L_{\text{total}} = \sum_{i \in \text{tag}} (\ln L_i^{\pi^+\pi^-\pi^+\pi^-} + \ln L_i^{\pi^+\pi^-\pi^0\pi^0}), \quad (39)$$

and the free parameters are optimized via a maximum likelihood fit using the MINUIT [49] package.

Generally, all the possible intermediate processes including the resonances listed in Table 7 and based on J^P conservation are considered in the fit. The only exception are D^0 decays, where parity conservation is not required. Only processes with a significance greater than 5σ are kept during the fit unless otherwise noted. Here, the significance of a specific amplitude is calculated according to the Wilks's Theorem by comparing the change of log-likelihood ($2\Delta \ln L$) to the expected values from the chi-square distribution ($\chi^2_{\Delta N_{\text{para}}}$) with the number of degrees of freedom (NDF) equal to the change of the numbers of fit parameters (ΔN_{para}). If the significance of the amplitudes containing the isospin vector in the 3π invariant mass spectrum is greater than 5σ , the corresponding isospin partners with significance greater than 3σ are also kept. For the P -vector of the $\pi\pi$ S-wave, only the parameters before the 1st and 2nd poles and $\pi\pi$, KK non-resonant terms are considered, and the others are fixed to zero in the nominal fit. Meanwhile, only those with significance greater than 3σ are kept.

To find the optimal solution, the baseline model containing the processes from Refs. [12, 13] is built up first. Next, starting from the baseline model, the significance of each possible process is tested, and the most significant among those satisfying the significance requirement is added to the current model. This step is repeated until no additional processes can be added. After this step, the significances of individual processes in the existing model are tested again, and those that do not satisfy the significance requirement are removed. The above steps are repeated until all the processes in the model satisfy the significance requirement, and no further ones can be added. The nominal amplitude model is obtained with this strategy and no multiple solutions are found.

Using the nominal amplitude model, the fit fraction (FF) of a specific amplitude i is calculated as

Table 7. Resonances considered in this analysis.

	$J^P = 0^+$	$J^P = 0^-$	$J^P = 1^+$	$J^P = 1^-$	$J^P = 2^+$	$J^P = 2^-$
$\pi\pi$	$(\pi\pi)_S$			$\rho(770)$	$f_2(1270)$	
					$\rho(1450)$	
	$\pi(1300)$	$a_1(1260)$	$\omega(782)$	$a_2(1320)$	$\pi_2(1670)$	
			$a_1(1420)$	$\phi(1020)$		
$\pi\pi\pi$			$a_1(1640)$	$\pi_1(1400)$		
			$h_1(1170)$	$\pi_1(1600)$		

$$\text{FF}_i = \frac{\int |\Lambda_i U_i(p)|^2 d\Phi}{\int |\sum_j \Lambda_j U_j(p)|^2 d\Phi}. \quad (40)$$

The FF of the interference between two amplitudes i and j ($j \neq i$) is calculated as

$$\text{FF}_{ij} = \frac{\int 2\text{Re}[\Lambda_i U_i(p) \Lambda_j^* U_j^*(p)] d\Phi}{\int |\sum_k \Lambda_k U_k(p)|^2 d\Phi}. \quad (41)$$

The CP -even fraction F_+ is calculated as

$$F_+^f = \frac{\int |A_f^+(p)|^2 d\Phi}{\int |A_f^+(p)|^2 + |A_f^-(p)|^2 d\Phi}, \quad (42)$$

where $A_f^\pm(p) = \frac{1}{\sqrt{2}}[A_f(p) \pm \bar{A}_f(p)]$ is the amplitude of the $D^0 \rightarrow f$ decay in a CP -even or CP -odd state. The FF results of different amplitudes are summarized in Tables 8, 9 and 10. The resonant parameters, masses, and widths of $a_1(1260)$ and $\pi(1300)$ are determined by the parameter scans, as shown in Fig. 5, which are compatible with the values from PDG. The fit fractions of the interference terms are summarized in Table 11. The fit results show large interferences among the dominant intermediate processes $D^0 \rightarrow a_1(1260)\pi$, $D^0 \rightarrow \pi(1300)\pi$, $D^0 \rightarrow \rho(770)\rho(770)$, and $D^0 \rightarrow 2(\pi\pi)_S$. The results for F_+ obtained in this analysis are presented in Table 12, which show good agreement with other measurements. In all the above tables, the mean values are obtained based on the output from the MINUIT fit, while the corresponding statistical uncertainties are estimated by the bootstrap method [50] based on the data since the weighted maximum likelihood fit is used, and the statistical uncertainties given by the inverse second derivative of the negative logarithmic likelihood are no longer asymptotically correct [51]. In the bootstrap method, the bootstrap samples are generated by repeatedly resampling the data set with replacement a thousand times, and both sPlot and amplitude analysis are performed for these samples. The width of the distribution of the estimated parameter values is used to estimate the parameter uncertainty. The comparisons between data and MC projection based on the nominal model for various invariant mass and angle distributions are shown in Figs. 6 and 7.

VII. SYSTEMATIC UNCERTAINTY OF THE AMPLITUDE ANALYSIS

The systematic uncertainties of the amplitude analysis result from two aspects. One is the experimental systematic uncertainty, including those from background estimation, detection efficiency over PHSP, and fit bias. Another is the model-dependent systematic uncertainty, including those from the resonance line shape, the radii of

Blatt-Weisskopf barrier factors, quantum correlation parameters, and extra amplitudes. The fit is performed with alternative conditions to estimate these uncertainties for each source, and the deviations from the nominal results are taken as the corresponding uncertainties. Table 12 and 13 summarize the systematic uncertainties on the magnitude and phase of the fit parameters in the unit of the statistical uncertainty, respectively. Table 15 summarized the systematic uncertainties on the FFs, resonance parameters, and CP -even fractions in the unit of the statistical uncertainty. The total systematic uncertainties are the square roots of the quadrature sums of the individual contributions. The individual uncertainties are obtained as follows:

- Background estimation

The sPlot technique is used to estimate the signal weight and background; the corresponding sources of systematic uncertainty are all the PDFs and the magnitudes of peaking backgrounds in BKGVI in the 2D fit on the M_{bc}^{tag} versus M_{bc}^{sig} distribution. To estimate the corresponding uncertainties, an alternative fit on the M_{bc}^{tag} versus M_{bc}^{sig} distribution is performed by varying the means and widths of two Gaussian functions by $\pm 1\sigma$ for the signal, varying the fixed parameters of the ARGUS function by $\pm 1\sigma$ for BKGII and BKGIII, changing the Student's function to the bifurcated Student's function with different n and σ on the left and right sides of the maximum value and two ARGUS functions to one ARGUS function on the $(M_{bc}^{\text{sig}} + M_{bc}^{\text{tag}})$ dimension for BKGIII, varying the means and widths of the bifurcated Gaussian functions by $\pm 1\sigma$ for BKGIV and BKGV, and varying the fixed peaking background yields in BKGVI by $\pm 1\sigma$ according to the estimated values in Table 2. The output results are used in the sPlot technique and amplitude analysis.

- Detection efficiency

The systematic uncertainties due to detection efficiencies are from the π^\pm tracking/PID and π^0 reconstruction. The corresponding uncertainties are obtained by weighting the PHSP signal MC sample with a factor $\epsilon_{\text{Data}}/\epsilon_{\text{MC}}$ when normalizing the PDF in the amplitude analysis, where ϵ_{Data} and ϵ_{MC} are the efficiencies of the data and MC simulation, respectively. The π^\pm tracking/PID efficiencies are quoted from Ref. [55], while the efficiency of the π^0 reconstruction is studied with the control samples of $D^0 \rightarrow K^-\pi^+\pi^0$ and $D^0 \rightarrow \pi^+\pi^-\pi^0$ versus the three tag modes used in this analysis.

- Fit bias

The sPlot technique, MC integration, detection resolution, and many other potential problems from fit tools may lead to fit bias. To estimate this fit bias, 100 sets of

Table 8. The fit parameters, FFs, and significances of individual amplitudes, where the first uncertainties are statistical, the second are the experimental systematic uncertainties and the third are the model-dependent systematic uncertainties.

Amplitude	Magnitude	Phase (rad)	FF (%)		Significance (σ)
			$\pi^+\pi^-\pi^+\pi^-$	$\pi^+\pi^-\pi^0\pi^0$	
$a_1(1260)^+\pi^-$	100(fixed)	0(fixed)	$82.2 \pm 3.3 \pm 2.3 \pm 15.8$	$57.4 \pm 2.7 \pm 3.0 \pm 6.5$	>10
$a_1(1260)^-\pi^+$	$35.3 \pm 2.7 \pm 0.8 \pm 4.6$	$0.23 \pm 0.07 \pm 0.02 \pm 0.16$	$10.3 \pm 1.5 \pm 0.3 \pm 2.5$	$7.2 \pm 1.1 \pm 0.2 \pm 2.2$	>10
$a_1(1260)^0\pi^0$	$50.9 \pm 3.1 \pm 0.4 \pm 4.7$	$-2.99 \pm 0.06 \pm 0.08 \pm 0.14$	—	$32.9 \pm 3.2 \pm 1.6 \pm 8.3$	>10
$a_1(1420)^+\pi^-$	$19.0 \pm 3.6 \pm 1.3 \pm 3.9$	$2.70 \pm 0.18 \pm 0.05 \pm 1.09$	$0.6 \pm 0.2 \pm 0.0 \pm 0.2$	$0.3 \pm 0.1 \pm 0.0 \pm 0.1$	6.0
$a_1(1640)^+\pi^-$	$20.1 \pm 3.0 \pm 2.6 \pm 5.8$	$-2.07 \pm 0.16 \pm 0.02 \pm 0.28$	$1.7 \pm 0.5 \pm 0.4 \pm 0.8$	$1.1 \pm 0.3 \pm 0.2 \pm 0.6$	7.3
$a_1(1640)^-\pi^+$	$10.5 \pm 2.8 \pm 0.6 \pm 3.8$	$-1.26 \pm 0.29 \pm 0.23 \pm 0.50$	$0.5 \pm 0.3 \pm 0.0 \pm 0.4$	$0.3 \pm 0.2 \pm 0.0 \pm 0.2$	5.2
$a_2(1320)^+\pi^-$	$0.23 \pm 0.07 \pm 0.03 \pm 0.05$	$-2.92 \pm 0.30 \pm 0.14 \pm 0.23$	$0.2 \pm 0.1 \pm 0.0 \pm 0.1$	$0.2 \pm 0.1 \pm 0.0 \pm 0.1$	4.6
$a_2(1320)^-\pi^+$	$0.30 \pm 0.05 \pm 0.01 \pm 0.04$	$-0.47 \pm 0.21 \pm 0.06 \pm 0.15$	$0.4 \pm 0.1 \pm 0.0 \pm 0.1$	$0.3 \pm 0.1 \pm 0.0 \pm 0.1$	6.4
$h_1(1170)^0\pi^0$	$9.7 \pm 2.2 \pm 1.5 \pm 3.6$	$-0.59 \pm 0.27 \pm 0.09 \pm 0.35$	—	$1.3 \pm 0.6 \pm 0.4 \pm 1.0$	6.5
$\pi(1300)^+\pi^-$	$76.3 \pm 3.6 \pm 4.6 \pm 4.3$	$-2.325 \pm 0.044 \pm 0.038 \pm 0.297$	$32.3 \pm 2.6 \pm 1.6 \pm 4.2$	$15.6 \pm 1.4 \pm 1.3 \pm 2.2$	>10
$\pi(1300)^-\pi^+$	$65.1 \pm 3.4 \pm 3.3 \pm 3.9$	$-2.631 \pm 0.045 \pm 0.083 \pm 0.208$	$23.5 \pm 2.3 \pm 0.5 \pm 3.9$	$11.4 \pm 1.1 \pm 0.6 \pm 2.3$	>10
$\pi(1300)^0\pi^0$	$61.1 \pm 3.2 \pm 3.3 \pm 4.0$	$0.61 \pm 0.05 \pm 0.08 \pm 0.29$	—	$23.2 \pm 2.8 \pm 1.4 \pm 3.1$	>10
$\pi_2(1670)^0\pi^0$	$12.2 \pm 1.5 \pm 1.5 \pm 2.1$	$-1.11 \pm 0.14 \pm 0.13 \pm 0.36$	—	$1.1 \pm 0.2 \pm 0.2 \pm 0.3$	6.9
$\rho(770)^0\rho(770)^0$	—	—	$28.0 \pm 1.9 \pm 0.6 \pm 3.0$	—	>10
[S]	$6.1 \pm 1.1 \pm 0.3 \pm 1.4$	$-3.10 \pm 0.17 \pm 0.11 \pm 0.50$	$1.7 \pm 0.6 \pm 0.1 \pm 0.5$	—	6.5
[P]	$6.17 \pm 0.36 \pm 0.13 \pm 0.58$	$1.62 \pm 0.07 \pm 0.02 \pm 0.09$	$9.8 \pm 1.0 \pm 0.4 \pm 0.8$	—	>10
[D]	$4.54 \pm 0.22 \pm 0.06 \pm 0.34$	$-3.06 \pm 0.05 \pm 0.01 \pm 0.20$	$23.1 \pm 2.1 \pm 0.8 \pm 2.3$	—	>10
$\rho(770)^0\rho(1450)^0$	—	—	$2.5 \pm 0.9 \pm 0.0 \pm 1.2$	—	8.0
[P]	$13.9 \pm 2.5 \pm 0.7 \pm 1.5$	$0.68 \pm 0.20 \pm 0.09 \pm 0.15$	$1.0 \pm 0.4 \pm 0.1 \pm 0.6$	—	6.4
[D]	$5.6 \pm 1.3 \pm 0.3 \pm 1.2$	$3.08 \pm 0.20 \pm 0.07 \pm 0.43$	$1.5 \pm 0.9 \pm 0.2 \pm 1.1$	—	5.0
$\rho(770)^+\rho(770)^-$	—	—	—	$90.9 \pm 3.9 \pm 3.5 \pm 6.6$	>10
[S]	$13.7 \pm 1.2 \pm 0.6 \pm 1.3$	$3.03 \pm 0.09 \pm 0.09 \pm 0.17$	—	$13.0 \pm 2.0 \pm 1.2 \pm 3.2$	>10
[P]	$7.10 \pm 0.36 \pm 0.23 \pm 0.35$	$-1.69 \pm 0.07 \pm 0.02 \pm 0.14$	—	$19.6 \pm 1.3 \pm 1.3 \pm 1.3$	>10
[D]	$4.59 \pm 0.22 \pm 0.05 \pm 0.24$	$0.06 \pm 0.05 \pm 0.02 \pm 0.09$	—	$36.0 \pm 3.0 \pm 0.6 \pm 2.4$	>10
$\rho(770)^+\rho(1450)^-[D]$	$8.1 \pm 1.7 \pm 1.4 \pm 2.7$	$-1.01 \pm 0.18 \pm 0.11 \pm 0.26$	—	$1.7 \pm 0.8 \pm 0.6 \pm 1.7$	6.3
$\rho(770)^0(\pi\pi)_S$	—	—	$2.7 \pm 0.6 \pm 0.3 \pm 1.7$	$1.0 \pm 0.2 \pm 0.1 \pm 0.4$	>10
β_1	$8.4 \pm 3.6 \pm 1.1 \pm 1.6$	$-1.68 \pm 0.50 \pm 0.26 \pm 0.29$	—	—	—
$f_{\pi\pi}^{\text{prod}}$	$40.7 \pm 5.0 \pm 3.7 \pm 3.9$	$-0.50 \pm 0.14 \pm 0.09 \pm 0.14$	—	—	—
f_{KK}^{prod}	$121 \pm 25 \pm 11 \pm 16$	$1.73 \pm 0.23 \pm 0.03 \pm 0.16$	—	—	—
$(\pi^+\pi^-)_S(\pi\pi)_S$	—	—	$62.8 \pm 4.6 \pm 0.5 \pm 9.7$	$37.4 \pm 3.0 \pm 1.8 \pm 4.8$	>10
$a_{1,1}$	$2224 \pm 35 \pm 26 \pm 33$	$-1.044 \pm 0.019 \pm 0.008 \pm 0.074$	—	—	—
$a_{1,2}$	$7287 \pm 62 \pm 46 \pm 93$	$1.727 \pm 0.009 \pm 0.004 \pm 0.062$	—	—	—
$b_{2,\pi\pi}$	$8816 \pm 120 \pm 181 \pm 90$	$-1.107 \pm 0.014 \pm 0.002 \pm 0.082$	—	—	—
$c_{[\pi\pi,\pi\pi]}$	$2433 \pm 96 \pm 67 \pm 90$	$1.796 \pm 0.043 \pm 0.042 \pm 0.044$	—	—	—
$c_{[\pi\pi,KK]}$	$5417 \pm 477 \pm 47 \pm 462$	$2.68 \pm 0.10 \pm 0.06 \pm 0.09$	—	—	—
$f_2(1270)^0(\pi\pi)_S$	—	—	$1.8 \pm 0.4 \pm 0.0 \pm 1.3$	$1.1 \pm 0.2 \pm 0.0 \pm 0.7$	9.1
$f_{\pi\pi}^{\text{prod}}$	$18.3 \pm 1.8 \pm 1.1 \pm 3.5$	$-1.39 \pm 0.10 \pm 0.04 \pm 0.20$	—	—	—
f_{KK}^{prod}	$56 \pm 10 \pm 14 \pm 8$	$2.29 \pm 0.20 \pm 0.05 \pm 0.39$	—	—	—
$\omega(782)\pi^0$	$1.58 \pm 0.30 \pm 0.05 \pm 0.13$	$-0.50 \pm 0.44 \pm 0.15 \pm 0.23$	—	$0.9 \pm 0.4 \pm 0.0 \pm 0.2$	6.1
$\phi(1020)\pi^0$	$0.44 \pm 0.06 \pm 0.03 \pm 0.05$	$2.51 \pm 0.41 \pm 0.10 \pm 0.22$	—	$1.5 \pm 0.4 \pm 0.2 \pm 0.2$	7.4

Table 9. The fit parameters, FFs and significance for the three-body decays of $a_1(1260)$, $a_1(1420)$, $a_1(1640)$, $a_2(1320)$, $h_1(1170)$, $\pi(1300)$, and $\pi_2(1670)$. The first uncertainties are the statistical uncertainties, the second are the experimental systematic uncertainties, and the third are the model-dependent systematic uncertainties.

Amplitude	Magnitude	Phase (rad)	Relative FF (%)			Significance (σ)
			$\pi^+\pi^-\pi^+\pi^-$		$\pi^+\pi^-\pi^0\pi^0$	
			charge = ±1	charge = ±1	charge = 0	
$a_1(1260) \rightarrow \rho(770)\pi[S]$	1(fixed)	0(fixed)	79.7±2.2±1.8±3.1	81.2±2.0±1.6±2.8	78.9±2.2±1.5±3.5	>10
$a_1(1260) \rightarrow \rho(770)\pi[D]$	0.060±0.009±0.002±0.022	0.01±0.17±0.09±0.09	1.3±0.3±0.1±0.7	1.2±0.3±0.1±0.6	1.3±0.3±0.1±0.7	7.5
$a_1(1260) \rightarrow f_2(1270)\pi[P]$	0.311±0.033±0.019±0.021	-1.58±0.11±0.08±0.25	1.8±0.4±0.3±0.5	0.8±0.2±0.1±0.3	1.2±0.2±0.1±0.3	>10
$a_1(1260) \rightarrow (\pi^+\pi^-)_S\pi[P]$	-	-	5.4±0.6±0.5±0.8	3.1±0.4±0.4±0.7	3.9±0.5±0.5±0.9	>10
β_1	0.83±0.13±0.11±0.34	-2.18±0.14±0.19±0.16	-	-	-	-
$f_{\pi\pi}^{\text{prod}}$	2.47±0.16±0.12±0.12	0.34±0.08±0.06±0.12	-	-	-	-
f_{KK}^{prod}	6.59±0.84±0.85±1.24	1.76±0.12±0.08±0.13	-	-	-	-
$\pi(1300) \rightarrow \rho(770)\pi$	1(fixed)	0(fixed)	53.8±2.9±0.9±8.7	79.0±2.0±0.8±6.8	73.6±2.6±0.8±9.1	>10
$\pi(1300) \rightarrow (\pi^+\pi^-)_S\pi$	-	-	51.1±2.9±0.9±8.4	26.2±2.1±0.8±6.5	36.7±2.6±1.0±8.3	>10
β_1	5.0±0.5±0.2±0.2	-0.64±0.10±0.04±0.25	-	-	-	-
f_{KK}^{prod}	43.8±2.8±0.5±2.7	0.34±0.06±0.02±0.06	-	-	-	-
$a_1(1420) \rightarrow f_0(980)\pi[P]$	1(fixed)	0(fixed)	100	100	-	6.0
$a_1(1640) \rightarrow \rho(770)\pi[S]$	1(fixed)	0(fixed)	100	100	-	9.1
$a_2(1320) \rightarrow \rho(770)\pi[D]$	1(fixed)	0(fixed)	100	100	-	7.3
$h_1(1170) \rightarrow \rho(770)\pi[S]$	1(fixed)	0(fixed)	-	-	100	6.5
$\pi_2(1670) \rightarrow f_2(1270)\pi[S]$	1(fixed)	0(fixed)	-	-	100	6.9

Table 10. Masses and widths of $a_1(1260)$ and $\pi(1300)$ obtained via parameter scans and presented in the PDG [25]. The first uncertainties in this fit are the statistical uncertainties, the second are the experimental systematic uncertainties, and the third are the model-dependent systematic uncertainties.

	This work		PDG	
	Mass/(GeV/ c^2)	Width/GeV	Mass/(GeV/ c^2)	Width/GeV
$a_1(1260)$	1.193±0.005±0.003±0.023	0.487±0.009±0.015±0.039	1.230±0.040	0.250–0.600
$\pi(1300)$	1.534±0.011±0.009±0.020	0.610±0.030±0.021±0.090	1.300±0.100	0.200–0.600

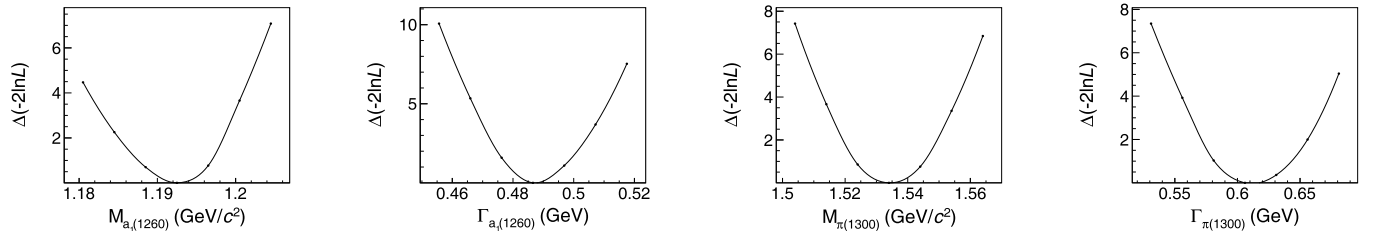


Fig. 5. Likelihood scans for masses and widths of $a_1(1260)$ and $\pi(1300)$.

samples with the same size and signal purity as the data are generated, where the signal events are generated according to the nominal model and the background events are from the inclusive MC sample. The amplitude fit is performed on these samples, and the average deviations of the fitted parameters from their input values are

taken as uncertainties due to fit bias.

- The resonance parameters and models

The systematic uncertainties associated with the masses and widths of resonances in the amplitude analysis are estimated by shifting the corresponding fixed PDG

Table 11. The fit fractions of interference terms in $D^0 \rightarrow \pi^+ \pi^- \pi^+ \pi^-$ (first) and $D^0 \rightarrow \pi^+ \pi^- \pi^0 \pi^0$ (second). The uncertainties are statistical only.

FF(%)	1	2	3	4	5	6	7	8	9	10	11	12	13	14						
1. $D^0 \rightarrow a_1(1260)^+ \pi^-$	82.2 ± 3.3	9.9 ± 0.8	0.5 ± 0.3	-15.3 ± 2.5	-0.4 ± 0.7	0.0 ± 0.0	0.0 ± 0.0	1.7 ± 0.2	-27.3 ± 2.1	-4.6 ± 1.9	-5.2 ± 1.5	-1.3 ± 2.3	5.2 ± 1.1	-1.4 ± 0.2						
2. $D^0 \rightarrow a_1(1260)^- \pi^+$	10.3 ± 1.5	-0.1 ± 0.1	-1.4 ± 0.3	-2.5 ± 0.8	0.0 ± 0.0	0.0 ± 0.0	-10.8 ± 1.2	-0.1 ± 0.1	-1.8 ± 0.7	-1.5 ± 0.5	-0.3 ± 0.8	3.4 ± 0.5	-0.4 ± 0.1							
3. $D^0 \rightarrow a_1(1420)^+ \pi^-$	0.6 ± 0.2	0.1 ± 0.1	-0.0 ± 0.0	0.0 ± 0.0	0.0 ± 0.0	-0.2 ± 0.0	0.1 ± 0.1	-0.3 ± 0.1	-0.1 ± 0.1	-0.2 ± 0.1	1.0 ± 0.2	-0.2 ± 0.0								
4. $D^0 \rightarrow a_1(1640)^+ \pi^-$	1.7 ± 0.5	0.2 ± 0.1	-0.0 ± 0.0	-0.0 ± 0.0	0.2 ± 0.1	4.9 ± 0.7	-1.1 ± 0.3	0.3 ± 0.1	0.1 ± 0.3	-1.6 ± 0.6	0.1 ± 0.0									
5. $D^0 \rightarrow a_1(1640)^- \pi^+$	0.5 ± 0.3	-0.0 ± 0.0	-0.0 ± 0.0	2.7 ± 0.8	0.3 ± 0.1	-0.2 ± 0.2	0.1 ± 0.1	0.4 ± 0.3	-1.9 ± 0.5	-0.0 ± 0.0										
6. $D^0 \rightarrow a_2(1320)^+ \pi^-$	0.2 ± 0.1	-0.1 ± 0.0	0.0 ± 0.0	0.0 ± 0.0	-0.8 ± 0.3	0.2 ± 0.1	-0.0 ± 0.0	-0.0 ± 0.0	-0.0 ± 0.0	-0.0 ± 0.0										
7. $D^0 \rightarrow a_2(1320)^- \pi^+$	0.3 ± 0.1	-0.0 ± 0.0	-0.0 ± 0.0	1.0 ± 0.2	-0.2 ± 0.1	0.0 ± 0.0	0.0 ± 0.0	0.0 ± 0.0	0.0 ± 0.0	0.0 ± 0.0										
8. $D^0 \rightarrow \pi(1300)^+ \pi^-$	32.3 ± 2.6	9.2 ± 1.5	-9.3 ± 0.7	-2.8 ± 0.8	4.0 ± 1.6	-49.2 ± 4.1	0.3 ± 0.3													
9. $D^0 \rightarrow \pi(1300)^- \pi^+$	23.5 ± 2.3	-6.0 ± 0.7	-2.6 ± 0.7	-2.8 ± 1.5	-39.8 ± 3.9	-0.1 ± 0.3														
10. $D^0 \rightarrow \rho(770)^0 \rho(770)^0$	28.0 ± 1.9	0.0 ± 2.1	0.0 ± 0.0	2.0 ± 0.5	2.5 ± 0.9	0.0 ± 0.0	-0.6 ± 0.3	-0.3 ± 0.1	-1.2 ± 0.2											
11. $D^0 \rightarrow \rho(770)^0 \rho(1450)^0$	2.7 ± 0.6	0.0 ± 0.0	-0.0 ± 0.0	2.7 ± 0.6	2.7 ± 0.6	0.0 ± 0.0	-0.0 ± 0.0	-0.0 ± 0.0	-0.0 ± 0.0											
12. $D^0 \rightarrow \rho(770)^0 (\pi\pi)_S$	62.8 ± 4.6	-1.3 ± 0.4	1.8 ± 0.4																	
13. $D^0 \rightarrow (\pi^+ \pi^-)_S (\pi\pi)_S$																				
14. $D^0 \rightarrow f_2(1270)^0 (\pi\pi)_S$																				
FF(%)	1	2	3	4	5	6	7	8	9	10	11	12	13	14	15	16	17	18	19	20
1. $D^0 \rightarrow a_1(1260)^+ \pi^-$	57.5±2.7	4.6±0.4	8.5±0.6	0.7±0.2	-10.2±1.7	-0.3±0.3	0.0±0.0	-0.0±0.0	-1.6±0.4	-0.0±0.0	0.8±0.1	-18.6±1.8	0.6±0.2	-33.5±1.8	-1.4±1.2	-1.8±0.3	2.4±0.8	-0.4±0.1	0.0±0.0	-0.0±0.0
2. $D^0 \rightarrow a_1(1260)^- \pi^+$	7.2±1.1	3.1±0.3	-0.0±0.0	-0.6±0.1	-1.8±0.5	-0.0±0.0	0.0±0.0	0.6±0.1	0.3±0.0	-0.0±0.0	-7.6±1.0	0.1±0.1	-12.1±1.1	0.4±0.1	0.6±0.1	2.0±0.4	-0.1±0.0	0.0±0.0	-0.0±0.0	
3. $D^0 \rightarrow a_1(1260)^0 \pi^0$	32.9±3.2	-0.1±0.0	-1.5±0.3	-0.2±0.3	0.0±0.0	0.0±0.0	0.0±0.0	0.0±0.0	-11.4±1.1	-12.0±1.0	0.7±0.1	0.3±0.1	-34.3±2.6	0.3±0.8	0.0±0.0	4.8±1.1	-0.3±0.1	-0.0±0.0	-0.0±0.0	
4. $D^0 \rightarrow a_1(1420)^+ \pi^-$	0.3±0.1	0.0±0.1	-0.0±0.0	-0.0±0.0	0.0±0.0	-0.0±0.0	0.0±0.0	0.1±0.0	-0.3±0.1	-0.0±0.0	-0.4±0.1	0.0±0.0	-0.1±0.0	0.7±0.1	0.0±0.0	-0.0±0.0	0.0±0.0			
5. $D^0 \rightarrow a_1(1640)^- \pi^+$	1.1±0.3	0.1±0.0	-0.0±0.0	0.0±0.0	0.3±0.1	-0.0±0.0	-0.1±0.0	3.7±0.6	0.0±0.0	3.0±0.5	0.2±0.1	0.1±0.0	-1.3±0.4	0.0±0.0	0.0±0.0	0.0±0.0	0.0±0.0			
6. $D^0 \rightarrow a_1(1640)^- \pi^+$	0.3±0.2	0.0±0.0	-0.0±0.0	-0.0±0.0	-0.1±0.0	0.0±0.0	1.7±0.5	0.0±0.0	1.1±0.4	-0.0±0.0	-0.0±0.0	-0.1±0.4	-0.4±0.4	-0.0±0.0	-0.0±0.0	-0.0±0.0	-0.0±0.0			
7. $D^0 \rightarrow a_2(1320)^+ \pi^-$	0.2±0.1	-0.0±0.0	0.0±0.0	0.0±0.0	-0.0±0.0	0.0±0.0	0.0±0.0	-0.6±0.2	0.0±0.0	0.0±0.0	-0.0±0.0	-0.0±0.0	-0.0±0.0	-0.0±0.0	-0.0±0.0	-0.0±0.0	-0.0±0.0			
8. $D^0 \rightarrow a_2(1320)^- \pi^+$	0.3±0.1	-0.0±0.0	0.0±0.0	-0.0±0.0	-0.0±0.0	0.0±0.0	1.0±0.2	0.0±0.0	-0.0±0.0	-0.0±0.0	-0.0±0.0	-0.0±0.0	-0.0±0.0	-0.0±0.0	-0.0±0.0	-0.0±0.0	-0.0±0.0			
9. $D^0 \rightarrow h_1(1170)^0 \pi^0$	1.3±0.6	1.5±0.5	-1.7±0.4	-0.0±0.0	0.0±0.0	0.0±0.0	0.1±0.1	0.3±0.2	0.0±0.0	-0.0±0.0	0.0±0.0	-0.0±0.0	-0.0±0.0	-0.0±0.0	-0.0±0.0	-0.0±0.0	-0.0±0.0			
10. $D^0 \rightarrow \pi(1300)^+ \pi^-$	15.6±1.4	4.2±0.4	-3.7±0.4	-0.2±0.0	-5.3±0.7	-1.4±0.7	1.1±0.2	-14.6±1.2	0.2±0.1	0.0±0.0	-0.0±0.0	-0.0±0.0	-0.0±0.0	-0.0±0.0	-0.0±0.0	-0.0±0.0	-0.0±0.0			
11. $D^0 \rightarrow \pi(1300)^- \pi^+$	11.4±1.1	-3.1±0.4	-0.1±0.0	-1.9±0.6	0.3±0.2	-1.0±0.2	-1.11±1.1	0.1±0.1	0.1±0.0	0.0±0.0	-0.0±0.0	-0.0±0.0	-0.0±0.0	-0.0±0.0	-0.0±0.0	-0.0±0.0	-0.0±0.0			
12. $D^0 \rightarrow \pi(1300)^0 \pi^0$	23.2±2.8	0.4±0.1	-5.3±1.2	-1.1±0.6	0.0±0.0	-21.5±2.2	0.2±0.2	-0.0±0.0	0.0±0.0	-0.0±0.0	-0.0±0.0	-0.0±0.0	-0.0±0.0	-0.0±0.0	-0.0±0.0	-0.0±0.0	-0.0±0.0			
13. $D^0 \rightarrow \pi_2(1670)^0 \pi^0$	1.1±0.2	-0.6±0.2	-0.0±0.0	0.0±0.0	-0.0±0.0	-0.0±0.0	-0.5±0.2	0.0±0.0	-0.5±0.2	0.0±0.0	-0.0±0.0	-0.0±0.0	-0.0±0.0	-0.0±0.0	-0.0±0.0	-0.0±0.0	-0.0±0.0			
14. $D^0 \rightarrow \rho(770)^+ \rho(770)^-$	90.9±3.9	-5.1±3.4	0.0±0.0	-2.1±1.0	-2.4±0.3	0.0±0.0	-0.0±0.0	-0.0±0.0	-0.0±0.0	-0.0±0.0	-0.0±0.0	-0.0±0.0	-0.0±0.0	-0.0±0.0	-0.0±0.0	-0.0±0.0	-0.0±0.0			
15. $D^0 \rightarrow \rho(770)^+ \rho(1450)^-[D]$	1.7±0.8	0.0±0.0	-1.0±0.3	0.2±0.1	-0.2±0.1	-0.0±0.0	-0.0±0.0	-0.0±0.0	-0.0±0.0	-0.0±0.0	-0.0±0.0	-0.0±0.0	-0.0±0.0	-0.0±0.0	-0.0±0.0	-0.0±0.0	-0.0±0.0			
16. $D^0 \rightarrow \rho(770)^0 \pi^0$	1.0±0.2	0.0±0.0	0.0±0.0	0.0±0.0	0.0±0.0	0.0±0.0	0.0±0.0	0.0±0.0	0.0±0.0	0.0±0.0	0.0±0.0	0.0±0.0	0.0±0.0	0.0±0.0	0.0±0.0	0.0±0.0	0.0±0.0			
17. $D^0 \rightarrow (\pi^+ \pi^-)_S (\pi\pi)_S$	37.4±3.0	-0.0±0.0	-0.0±0.0	-0.0±0.0	-0.0±0.0	-0.0±0.0	-0.0±0.0	-0.0±0.0	-0.0±0.0	-0.0±0.0	-0.0±0.0	-0.0±0.0	-0.0±0.0	-0.0±0.0	-0.0±0.0	-0.0±0.0	-0.0±0.0			
18. $D^0 \rightarrow f_2(1270)^0 (\pi\pi)_S$	1.1±0.2	0.0±0.0	0.0±0.0	-0.0±0.0	-0.0±0.0	-0.0±0.0	-0.0±0.0	-0.0±0.0	-0.0±0.0	-0.0±0.0	-0.0±0.0	-0.0±0.0	-0.0±0.0	-0.0±0.0	-0.0±0.0	-0.0±0.0	-0.0±0.0			
19. $D^0 \rightarrow \omega(782)^0 \pi^0$	0.9±0.4	-0.0±0.0	-0.0±0.0	-0.0±0.0	-0.0±0.0	-0.0±0.0	-0.0±0.0	-0.0±0.0	-0.0±0.0	-0.0±0.0	-0.0±0.0	-0.0±0.0	-0.0±0.0	-0.0±0.0	-0.0±0.0	-0.0±0.0	-0.0±0.0			
20. $D^0 \rightarrow \phi(1020)\pi^0$	1.5±0.4	-0.0±0.0	-0.0±0.0	-0.0±0.0	-0.0±0.0	-0.0±0.0	-0.0±0.0	-0.0±0.0	-0.0±0.0	-0.0±0.0	-0.0±0.0	-0.0±0.0	-0.0±0.0	-0.0±0.0	-0.0±0.0	-0.0±0.0	-0.0±0.0			

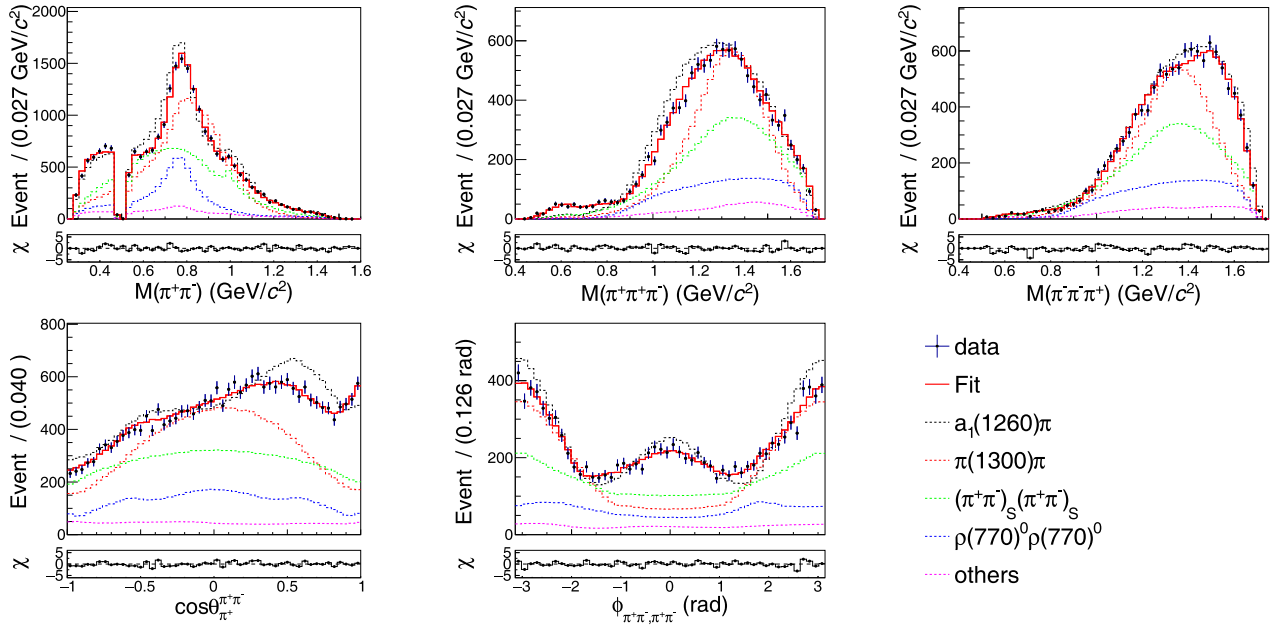


Fig. 6. (color online) The mass and angular distributions for $D^0 \rightarrow \pi^+\pi^-\pi^+\pi^-$, where θ_a^{ab} is the helicity angle of a in the ab system, $\phi_{ab,cd}$ is the angle between the decay planes of the ab and cd systems in the D^0 rest frame.

Table 12. The CP -even fractions obtained in this work and comparisons with the CLEO-c and prior BESIII measurements.

	$F_+^{\pi^+\pi^-\pi^+\pi^-}$	$F_+^{\pi^+\pi^-\pi^0\pi^0}$ (non- η)
This work (model-dependent)	$(75.2 \pm 1.1_{\text{stat.}} \pm 1.5_{\text{syst.}})\%$	$(68.9 \pm 1.5_{\text{stat.}} \pm 2.4_{\text{syst.}})\%$
CLEO-c (model-dependent)	$(72.9 \pm 0.9_{\text{stat.}} \pm 1.5_{\text{syst.}} \pm 1.0_{\text{model}})\%$ [13]	–
CLEO-c (model-independent, global)	$(73.7 \pm 2.8)\%$ [52]	–
CLEO-c (model-independent, binned)	$(76.9 \pm 2.1_{\text{stat.}} \pm 1.0_{\text{syst.}} \pm 0.2_{K_S \text{ veto}})\%$ [6]	–
BESIII (model-independent, global)	$(73.4 \pm 1.5_{\text{stat.}} \pm 0.8_{\text{syst.}})\%$ [53]	$(68.2 \pm 7.7)\%$ [54]

[25] values or optimized values by $\pm 1\sigma$. The systematic uncertainties associated with the model of $\pi\pi$ S-wave are estimated by replacing the K -matrix formula with the sum of three independent resonances of $f_0(500)$, $f_0(980)$, and $f_0(1370)$, described by the formula in Ref. [56], a Flatté parametrization, and a relative Breit-Wigner function. For the magnitude and phase of the fit parameters of $\pi\pi$ S-wave, the systematic uncertainties associated with the $\pi\pi$ S-wave model are not considered. The overall uncertainties are the square roots of the quadrature sums of the individual contributions.

• Radii of Blatt-Weisskopf barrier factors

The systematic uncertainties due to the radii of Blatt-Weisskopf barrier factors are obtained by varying the radii of the D^0 meson and other resonances by $\pm 1 \text{ GeV}^{-1}c$ in the amplitude analysis, and the square root of the quadrature sum of the individual effects is taken as the uncertainty. The radii choice significantly affects the magnitudes of the fit parameters, especially for the components with high orbital angular momentum. Therefore, this part is not included in the systematic uncertainties of

the magnitudes of the fit parameters.

• Quantum correlation correction

The systematic uncertainty due to the quantum correlation correction is estimated by varying the input quantum correlation parameters by $\pm 1\sigma$ in the amplitude analysis.

• Extra amplitudes

The systematic uncertainties due to the extra amplitudes are estimated with the alternative fits with the models, including an additional amplitude of $f_2(1270)f_2(1270)[D]$ or $1^{++}[\rho(770)^+\pi^-[S]]_{\text{NR}}\pi^0$ ("NR" represents non-resonant contribution), which are of 3σ to 5σ significance based on the nominal model. The square root of the quadrature sum of the individual effects is taken as the uncertainty.

VIII. MEASUREMENT OF BRANCHING FRACTIONS

The absolute branching fractions of $D^0 \rightarrow \pi^+\pi^-\pi^+\pi^-$

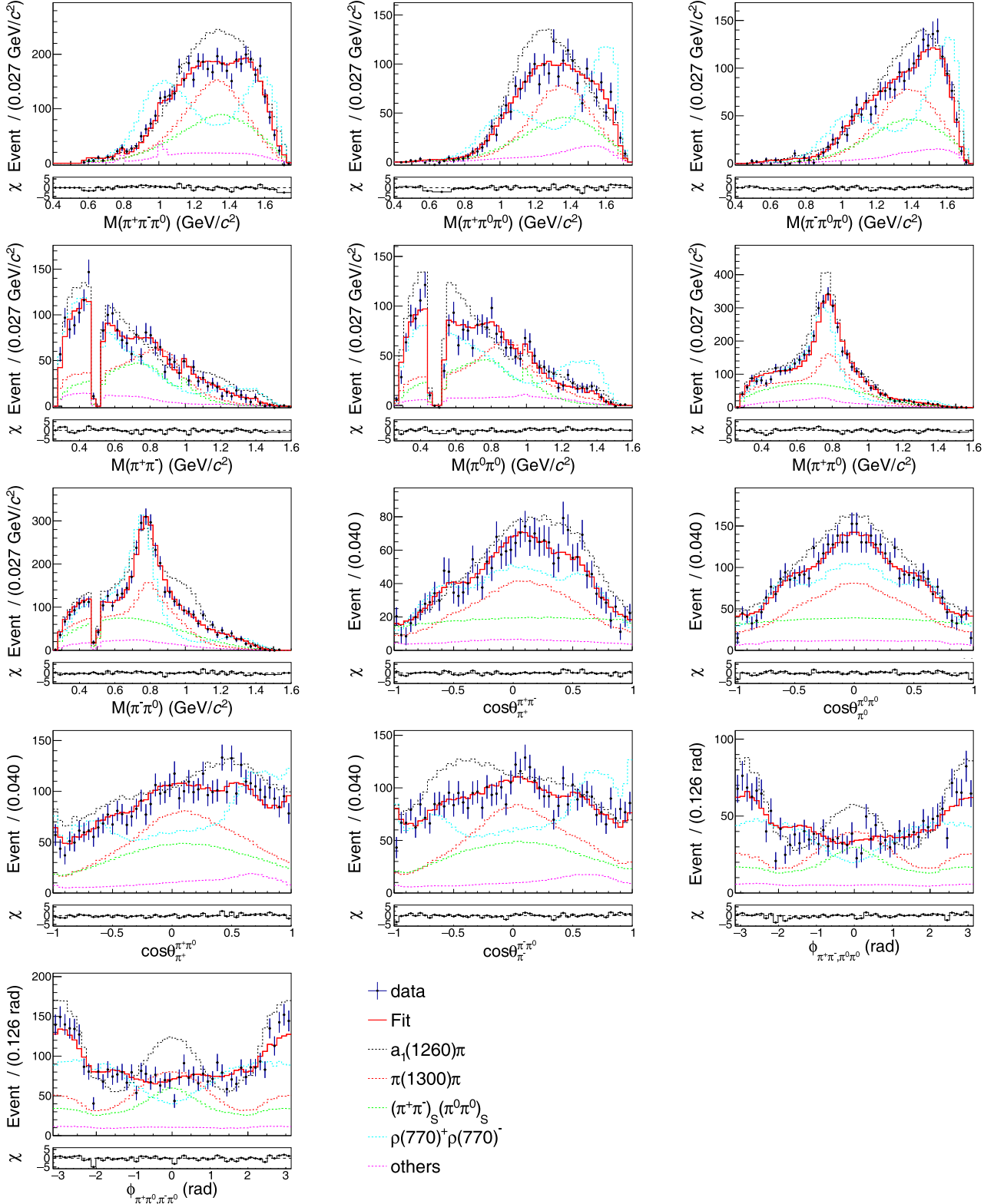


Fig. 7. (color online) The mass and angular distributions in $D^0 \rightarrow \pi^+\pi^-\pi^0\pi^0$, where θ_a^{ab} is the helicity angle of a in the ab system and $\phi_{ab,cd}$ is the angle between the decay planes of the ab and cd systems in the D^0 rest frame.

Table 13. Systematic uncertainties in the magnitude of fit parameters in units of statistical standard deviations. 1: Background estimation. 2: Detection efficiency. 3: Fit bias. 4: Resonance parameters. 5: Radii of Blatt-Weisskopf barrier factors. 6: Quantum correlation correction. 7: Extra amplitudes. In the "Total" column, the term before " \pm " is the total experimental systematic uncertainty (1, 2, and 3), and the term after " \pm " is the total model-dependent systematic uncertainty (4, 5, 6, and 7). The systematic uncertainties from "5" are not considered here.

	1	2	3	4	5	6	7	Total
magnitude($D^0 \rightarrow a_1(1260)^-\pi^+$)	0.2	0.1	0.2	1.6	—	0.1	0.7	0.3 ± 1.7
magnitude($D^0 \rightarrow a_1(1260)^0\pi^0$)	0.1	0.0	0.1	1.3	—	0.0	0.8	0.1 ± 1.5
magnitude($D^0 \rightarrow a_1(1420)^+\pi^-$)	0.2	0.0	0.3	1.0	—	0.1	0.5	0.4 ± 1.1
magnitude($D^0 \rightarrow a_1(1640)^+\pi^-$)	0.8	0.2	0.2	1.4	—	0.2	1.3	0.9 ± 1.9
magnitude($D^0 \rightarrow a_1(1640)^-\pi^+$)	0.1	0.1	0.2	0.6	—	0.2	1.2	0.2 ± 1.4
magnitude($D^0 \rightarrow a_2(1320)^+\pi^-$)	0.2	0.1	0.3	0.7	—	0.1	0.2	0.4 ± 0.7
magnitude($D^0 \rightarrow a_2(1320)^-\pi^+$)	0.0	0.0	0.2	0.6	—	0.1	0.5	0.2 ± 0.8
magnitude($D^0 \rightarrow h_1(1170)^0\pi^0$)	0.6	0.1	0.1	1.3	—	0.0	1.0	0.7 ± 1.7
magnitude($D^0 \rightarrow \pi(1300)^+\pi^-$)	1.3	0.0	0.0	1.1	—	0.1	0.4	1.3 ± 1.2
magnitude($D^0 \rightarrow \pi(1300)^-\pi^+$)	0.8	0.1	0.6	1.1	—	0.1	0.1	1.0 ± 1.1
magnitude($D^0 \rightarrow \pi(1300)^0\pi^0$)	1.0	0.2	0.1	1.2	—	0.2	0.3	1.0 ± 1.2
magnitude($D^0 \rightarrow \pi_2(1670)^0\pi^0$)	0.7	0.1	0.6	0.3	—	0.1	1.4	1.0 ± 1.4
magnitude($D^0 \rightarrow \rho(770)^0\rho(770)^0[S]$)	0.0	0.0	0.3	1.2	—	0.0	0.4	0.3 ± 1.3
magnitude($D^0 \rightarrow \rho(770)^0\rho(770)^0[P]$)	0.3	0.0	0.2	1.5	—	0.4	0.4	0.4 ± 1.6
magnitude($D^0 \rightarrow \rho(770)^0\rho(770)^0[D]$)	0.1	0.0	0.2	1.5	—	0.0	0.2	0.3 ± 1.5
magnitude($D^0 \rightarrow \rho(770)^0\rho(1450)^0[P]$)	0.0	0.2	0.2	0.5	—	0.3	0.2	0.3 ± 0.6
magnitude($D^0 \rightarrow \rho(770)^0\rho(1450)^0[D]$)	0.2	0.1	0.1	0.3	—	0.1	0.9	0.2 ± 0.9
magnitude($D^0 \rightarrow \rho(770)^+\rho(770)^-[S]$)	0.5	0.1	0.1	0.6	—	0.1	0.9	0.5 ± 1.1
magnitude($D^0 \rightarrow \rho(770)^+\rho(770)^-[P]$)	0.6	0.1	0.0	0.7	—	0.0	0.6	0.6 ± 1.0
magnitude($D^0 \rightarrow \rho(770)^+\rho(770)^-[D]$)	0.2	0.1	0.1	0.9	—	0.0	0.6	0.2 ± 1.1
magnitude($D^0 \rightarrow \rho(770)^+\rho(1450)^-[D]$)	0.8	0.1	0.1	1.4	—	0.1	0.7	0.8 ± 1.6
magnitude($D^0 \rightarrow \rho(770)^0(\pi\pi)_S, \beta_1$)	0.2	0.0	0.2	0.2	—	0.0	0.4	0.3 ± 0.4
magnitude($D^0 \rightarrow \rho(770)^0(\pi\pi)_S, f_{\pi\pi}^{\text{prod}}$)	0.6	0.0	0.4	0.4	—	0.1	0.7	0.7 ± 0.8
magnitude($D^0 \rightarrow \rho(770)^0(\pi\pi)_S, f_{KK}^{\text{prod}}$)	0.4	0.0	0.0	0.2	—	0.1	0.6	0.4 ± 0.7
magnitude($D^0 \rightarrow (\pi^+\pi^-)_S(\pi\pi)_S, a_{1,1}$)	0.7	0.1	0.0	0.5	—	0.1	0.8	0.7 ± 0.9
magnitude($D^0 \rightarrow (\pi^+\pi^-)_S(\pi\pi)_S, a_{1,2}$)	0.6	0.2	0.3	1.2	—	0.2	0.9	0.7 ± 1.5
magnitude($D^0 \rightarrow (\pi^+\pi^-)_S(\pi\pi)_S, b_{2,\pi\pi}$)	1.5	0.0	0.0	0.3	—	0.1	0.7	1.5 ± 0.7
magnitude($D^0 \rightarrow (\pi^+\pi^-)_S(\pi\pi)_S, c_{[\pi\pi,\pi\pi]}$)	0.6	0.1	0.2	0.4	—	0.1	0.8	0.7 ± 0.9
magnitude($D^0 \rightarrow (\pi^+\pi^-)_S(\pi\pi)_S, c_{[\pi\pi,KK]}$)	0.1	0.0	0.1	0.6	—	0.2	0.8	0.1 ± 1.0
magnitude($D^0 \rightarrow f_2(1270)^0(\pi\pi)_S, f_{\pi\pi}^{\text{prod}}$)	0.5	0.0	0.3	0.4	—	0.1	1.9	0.6 ± 1.9
magnitude($D^0 \rightarrow f_2(1270)^0(\pi\pi)_S, f_{KK}^{\text{prod}}$)	1.2	0.1	0.7	0.3	—	0.1	0.7	1.4 ± 0.8
magnitude($D^0 \rightarrow \omega(782)\pi^0$)	0.1	0.0	0.1	0.2	—	0.0	0.4	0.2 ± 0.4
magnitude($D^0 \rightarrow \phi(1020)\pi^0$)	0.2	0.1	0.4	0.6	—	0.1	0.5	0.5 ± 0.8
magnitude($a_1(1260) \rightarrow \rho(770)\pi[D]$)	0.1	0.0	0.1	2.4	—	0.0	0.2	0.2 ± 2.4
magnitude($a_1(1260) \rightarrow f_2(1270)\pi[P]$)	0.6	0.0	0.1	0.5	—	0.1	0.3	0.6 ± 0.6
magnitude($a_1(1260) \rightarrow (\pi^+\pi^-)_S\pi[P], \beta_1$)	0.9	0.0	0.0	0.6	—	0.0	2.5	0.9 ± 2.6
magnitude($a_1(1260) \rightarrow (\pi^+\pi^-)_S\pi[P], f_{\pi\pi}^{\text{prod}}$)	0.7	0.0	0.0	0.7	—	0.1	0.2	0.7 ± 0.7
magnitude($a_1(1260) \rightarrow (\pi^+\pi^-)_S\pi[P], f_{KK}^{\text{prod}}$)	1.0	0.0	0.2	0.8	—	0.1	1.3	1.0 ± 1.5
magnitude($\pi(1300) \rightarrow (\pi^+\pi^-)_S\pi, \beta_1$)	0.2	0.1	0.3	0.4	—	0.0	0.1	0.3 ± 0.5
magnitude($\pi(1300) \rightarrow (\pi^+\pi^-)_S\pi, f_{KK}^{\text{prod}}$)	0.2	0.0	0.1	0.8	—	0.1	0.5	0.2 ± 1.0

Table 14. Systematic uncertainties in the phase of fit parameters in units of statistical standard deviations. 1: Background estimation. 2: Detection efficiency. 3: Fit bias. 4: Resonance parameters. 5: Radii of Blatt-Weisskopf barrier factors. 6: Quantum correlation correction. 7: Extra amplitudes. In the "Total" column, the term before " \pm " is the total experimental systematic uncertainty (1, 2, and 3), and the term after " \pm " is the total model-dependent systematic uncertainty (4, 5, 6, and 7).

	1	2	3	4	5	6	7	Total
phase($D^0 \rightarrow a_1(1260)^- \pi^+$)	0.2	0.0	0.0	2.2	0.2	0.1	0.2	0.2 ± 2.2
phase($D^0 \rightarrow a_1(1260)^0 \pi^0$)	1.4	0.1	0.1	0.7	1.8	0.0	1.3	1.4 ± 2.3
phase($D^0 \rightarrow a_1(1420)^+ \pi^-$)	0.0	0.0	0.3	6.0	0.6	0.0	0.6	0.3 ± 6.1
phase($D^0 \rightarrow a_1(1640)^+ \pi^-$)	0.0	0.0	0.1	1.6	0.6	0.0	0.2	0.1 ± 1.7
phase($D^0 \rightarrow a_1(1640)^- \pi^+$)	0.8	0.0	0.2	1.1	1.2	0.2	0.6	0.8 ± 1.7
phase($D^0 \rightarrow a_2(1320)^+ \pi^-$)	0.5	0.1	0.1	0.6	0.2	0.0	0.5	0.5 ± 0.8
phase($D^0 \rightarrow a_2(1320)^- \pi^+$)	0.3	0.0	0.0	0.5	0.3	0.1	0.4	0.3 ± 0.7
phase($D^0 \rightarrow h_1(1170)^0 \pi^0$)	0.3	0.1	0.2	0.4	0.5	0.1	1.1	0.3 ± 1.3
phase($D^0 \rightarrow \pi(1300)^+ \pi^-$)	0.9	0.0	0.0	6.2	2.4	0.1	1.3	0.9 ± 6.8
phase($D^0 \rightarrow \pi(1300)^- \pi^+$)	1.8	0.1	0.1	3.6	2.5	0.0	1.4	1.9 ± 4.6
phase($D^0 \rightarrow \pi(1300)^0 \pi^0$)	1.6	0.1	0.0	5.1	2.2	0.1	1.6	1.6 ± 5.8
phase($D^0 \rightarrow \pi_2(1670)^0 \pi^0$)	0.9	0.0	0.0	1.7	0.6	0.1	1.8	0.9 ± 2.6
phase($D^0 \rightarrow \rho(770)^0 \rho(770)^0 [S]$)	0.6	0.0	0.1	2.9	0.6	0.2	0.4	0.6 ± 2.9
phase($D^0 \rightarrow \rho(770)^0 \rho(770)^0 [P]$)	0.1	0.2	0.1	1.2	0.0	0.2	0.5	0.2 ± 1.3
phase($D^0 \rightarrow \rho(770)^0 \rho(770)^0 [D]$)	0.2	0.0	0.1	3.7	0.7	0.1	1.0	0.2 ± 3.9
phase($D^0 \rightarrow \rho(770)^0 \rho(1450)^0 [P]$)	0.4	0.2	0.1	0.7	0.1	0.1	0.1	0.4 ± 0.8
phase($D^0 \rightarrow \rho(770)^0 \rho(1450)^0 [D]$)	0.4	0.0	0.0	1.7	1.0	0.2	0.6	0.4 ± 2.1
phase($D^0 \rightarrow \rho(770)^+ \rho(770)^- [S]$)	1.0	0.0	0.1	0.3	0.8	0.1	1.7	1.0 ± 1.9
phase($D^0 \rightarrow \rho(770)^+ \rho(770)^- [P]$)	0.1	0.1	0.3	1.8	0.8	0.2	0.4	0.3 ± 2.1
phase($D^0 \rightarrow \rho(770)^+ \rho(770)^- [D]$)	0.4	0.0	0.1	1.7	0.1	0.1	0.4	0.4 ± 1.8
phase($D^0 \rightarrow \rho(770)^+ \rho(1450)^- [D]$)	0.6	0.1	0.0	1.0	0.9	0.0	0.5	0.6 ± 1.4
phase($D^0 \rightarrow \rho(770)^0 (\pi\pi)_S, \beta_1$)	0.5	0.1	0.2	0.1	0.5	0.0	0.3	0.5 ± 0.6
phase($D^0 \rightarrow \rho(770)^0 (\pi\pi)_S, f_{\pi\pi}^{\text{prod}}$)	0.6	0.0	0.2	0.3	0.3	0.0	0.9	0.6 ± 1.0
phase($D^0 \rightarrow \rho(770)^0 (\pi\pi)_S, f_{KK}^{\text{prod}}$)	0.1	0.0	0.0	0.2	0.5	0.0	0.3	0.1 ± 0.7
phase($D^0 \rightarrow (\pi^+ \pi^-)_S (\pi\pi)_S, a_{1,1}$)	0.4	0.0	0.1	0.4	3.8	0.0	0.5	0.4 ± 3.9
phase($D^0 \rightarrow (\pi^+ \pi^-)_S (\pi\pi)_S, a_{1,2}$)	0.4	0.0	0.0	1.0	6.6	0.1	1.5	0.4 ± 6.9
phase($D^0 \rightarrow (\pi^+ \pi^-)_S (\pi\pi)_S, b_{2,\pi\pi}$)	0.1	0.0	0.0	0.4	5.6	0.1	1.5	0.2 ± 5.8
phase($D^0 \rightarrow (\pi^+ \pi^-)_S (\pi\pi)_S, c_{[\pi\pi,\pi\pi]}$)	1.0	0.0	0.1	0.3	0.7	0.0	0.7	1.0 ± 1.0
phase($D^0 \rightarrow (\pi^+ \pi^-)_S (\pi\pi)_S, c_{[\pi\pi,KK]}$)	0.4	0.0	0.3	0.5	0.5	0.1	0.6	0.6 ± 0.9
phase($D^0 \rightarrow f_2(1270)^0 (\pi\pi)_S, f_{\pi\pi}^{\text{prod}}$)	0.4	0.1	0.1	0.4	1.4	0.0	1.3	0.4 ± 2.0
phase($D^0 \rightarrow f_2(1270)^0 (\pi\pi)_S, f_{KK}^{\text{prod}}$)	0.2	0.0	0.2	0.3	1.6	0.1	1.1	0.2 ± 2.0
phase($D^0 \rightarrow \omega(782) \pi^0$)	0.3	0.0	0.1	0.5	0.3	0.0	0.0	0.3 ± 0.5
phase($D^0 \rightarrow \phi(1020) \pi^0$)	0.1	0.0	0.2	0.3	0.4	0.0	0.1	0.2 ± 0.5
phase($a_1(1260) \rightarrow \rho(770) \pi [D]$)	0.5	0.1	0.1	0.4	0.3	0.1	0.0	0.5 ± 0.5
phase($a_1(1260) \rightarrow f_2(1270) \pi [P]$)	0.7	0.0	0.1	2.2	0.2	0.0	0.7	0.7 ± 2.3
phase($a_1(1260) \rightarrow (\pi^+ \pi^-)_S \pi [P], \beta_1$)	1.3	0.2	0.3	0.6	0.9	0.2	0.3	1.4 ± 1.1
phase($a_1(1260) \rightarrow (\pi^+ \pi^-)_S \pi [P], f_{\pi\pi}^{\text{prod}}$)	0.7	0.1	0.1	0.5	0.5	0.1	1.2	0.7 ± 1.5
phase($a_1(1260) \rightarrow (\pi^+ \pi^-)_S \pi [P], f_{KK}^{\text{prod}}$)	0.6	0.0	0.0	0.3	0.4	0.1	0.9	0.6 ± 1.0
phase($\pi(1300) \rightarrow (\pi^+ \pi^-)_S \pi, \beta_1$)	0.3	0.1	0.2	0.3	2.4	0.1	0.8	0.4 ± 2.5
phase($\pi(1300) \rightarrow (\pi^+ \pi^-)_S \pi, f_{KK}^{\text{prod}}$)	0.2	0.0	0.2	0.5	0.3	0.1	0.8	0.3 ± 1.0

and $D^0 \rightarrow \pi^+ \pi^- \pi^0 \pi^0$ (non- η) are measured using the DT method. The numbers of ST events (N_g^{ST}) for the tag mode g and DT events (N_{fg}^{DT}) for the self-conjugated signal model f with the tag mode g are given by

$$N_g^{\text{ST}} = 2N_{D^0\bar{D}^0}\mathcal{B}_g\epsilon_g^{\text{ST}}(1+y_D^2)(1+r_g^2-2r_gR_gy_D\cos\delta_g), \quad (43)$$

$$N_{fg}^{\text{DT}} = 2N_{D^0\bar{D}^0}\mathcal{B}_f\mathcal{B}_g\epsilon_{fg}^{\text{DT}}(1+y_D^2)[1+r_g^2-2r_gR_g\cos\delta_g(2F_+^f-1)]. \quad (44)$$

Here, $N_{D^0\bar{D}^0}$ is the total number of $D^0\bar{D}^0$ pairs in the data, \mathcal{B}_f and \mathcal{B}_g are the branching fractions of the signal mode f and tag mode g , respectively, ϵ_f^{ST} and $\epsilon_{fg}^{\text{ST}}$ are the corresponding ST and DT efficiencies, and y_D is the $D^0\bar{D}^0$ mixing parameter. By combining Eqs. (43) and (44) and ignoring the term $2r_gR_gy_D\cos\delta_g$ in Eq. (43), the branching fraction of $D^0 \rightarrow f$ is given as

$$\mathcal{B}_f = \frac{\sum_g N_{fg}^{\text{DT}}}{\sum_g N_g^{\text{ST}}(\epsilon_{fg}^{\text{DT}}/\epsilon_g^{\text{ST}})\left[1 - \frac{2r_gR_g\cos\delta_g}{1+r_g^2}(2F_+^f-1)\right]}. \quad (45)$$

As described in Sec. IV, the ST and DT yields are extracted by performing an unbinned maximum likelihood fit on the M_{bc}^{tag} distribution and the 2D distribution of M_{bc}^{tag} versus M_{bc}^{sig} , respectively. The corresponding ST and DT efficiencies are obtained with the similar fit processes on the signal MC sample, as described in Sec. II. The corresponding ST and DT yields and the ST and DT efficiencies are summarized in Table 3. According to Eq. (45), the values in Table 3 and the CP -even fractions obtained in the amplitude analysis, the branching fractions of $D^0 \rightarrow \pi^+ \pi^- \pi^+ \pi^-$ and $D^0 \rightarrow \pi^+ \pi^- \pi^0 \pi^0$ (non- η) are calculated and summarized in Table 16. According to the FFs obtained in the amplitude analysis, the branching frac-

tions of the intermediate processes are also determined. The obtained results are summarized in Table 17.

Benefiting from the DT method, most systematic uncertainties associated with the ST selection are canceled. The relative systematic uncertainties in the branching fraction measurement are summarized in Table 18, where the total uncertainties are the square roots of the quadrature sums of the individual ones. Details of the systematic uncertainties in the branching fraction measurements are described below.

- Tracking efficiency

The tracking efficiency of π^\pm has been studied in Ref. [55]. The systematic uncertainties are assigned by re-weighting the data-MC difference in π^\pm tracking efficiencies according to the momentum distribution of π^\pm in the signal MC sample. They are assigned as 0.4% and 0.2% for $D^0 \rightarrow \pi^+ \pi^- \pi^+ \pi^-$ and $D^0 \rightarrow \pi^+ \pi^- \pi^0 \pi^0$, respectively.

- PID efficiency

The PID efficiency of π^\pm has been studied in Ref. [55]. The systematic uncertainties are assigned by re-weighting the data-MC difference in π^\pm PID efficiencies according to the momentum distribution of π^\pm in the signal MC sample. They are assigned as 1.2% and 0.6% for $D^0 \rightarrow \pi^+ \pi^- \pi^+ \pi^-$ and $D^0 \rightarrow \pi^+ \pi^- \pi^0 \pi^0$, respectively.

- π^0 reconstruction efficiency

The π^0 reconstruction efficiency is studied by the control samples $\bar{D}^0 \rightarrow K^+ \pi^-$, $K^+ \pi^- \pi^0$, $K^+ \pi^- \pi^+ \pi^-$ versus $D^0 \rightarrow K^- \pi^+ \pi^0$, $\pi^+ \pi^- \pi^0$. The corresponding systematic uncertainty for $D^0 \rightarrow \pi^+ \pi^- \pi^0 \pi^0$ is assigned as 1.3%, by re-weighting the data-MC difference in π^0 reconstruction efficiencies according to the momentum distribution of π^0 in the signal MC sample.

- ΔE requirement of the signal side

To study the systematic uncertainty from the ΔE requirement of the signal side, the ΔE of the signal MC

Table 15. Systematic uncertainties in the FFs, resonance parameters, and CP -even fractions in units of statistical standard deviations. 1: Background estimation. 2: Detection efficiency. 3: Fit bias. 4: Resonance parameters. 5: Radii of Blatt-Weisskopf barrier factors. 6: Quantum correlation correction. 7: Extra amplitudes. For the items with "/", the quantities before and after "/" are for $D^0 \rightarrow \pi^+ \pi^- \pi^+ \pi^-$ and $D^0 \rightarrow \pi^+ \pi^- \pi^0 \pi^0$, respectively. In the "Total" column, the term before " \pm " is the total experimental systematic uncertainty (1, 2, and 3), and the term after " \pm " is the total model-dependent systematic uncertainty (4, 5, 6, and 7).

	1	2	3	4	5	6	7	Total
FF($D^0 \rightarrow a_1(1260)^+\pi^-$)	0.6/1.1	0.0/0.1	0.3/0.1	3.8/0.5	3.0/2.1	0.0/0.1	0.2/1.1	$0.7 \pm 4.8/1.1 \pm 2.4$
FF($D^0 \rightarrow a_1(1260)^-\pi^+$)	0.1/0.1	0.1/0.1	0.2/0.2	0.7/1.5	1.4/1.2	0.1/0.1	0.7/0.7	$0.2 \pm 1.7/0.2 \pm 2.0$
FF($D^0 \rightarrow a_1(1260)^0\pi^0$)	-/0.4	-/0.1	-/0.2	-/1.8	-/1.7	-/0.0	-/0.9	$-/0.5 \pm 2.6$
FF($D^0 \rightarrow a_1(1420)^+\pi^-$)	0.1/0.2	0.0/0.0	0.1/0.0	0.4/0.7	0.4/0.5	0.0/0.1	0.6/0.5	$0.1 \pm 0.8/0.2 \pm 1.0$
FF($D^0 \rightarrow a_1(1640)^+\pi^-$)	0.7/0.8	0.2/0.2	0.2/0.1	0.6/0.9	1.1/1.1	0.2/0.2	1.2/1.3	$0.8 \pm 1.7/0.8 \pm 1.9$

Continued on next page

Table 15-continued from previous

	1	2	3	4	5	6	7	Total
FF($D^0 \rightarrow a_1(1640)^- \pi^+$)	0.1/0.1	0.1/0.1	0.0/0.0	0.4/0.2	0.6/0.6	0.2/0.2	0.9/1.0	$0.1 \pm 1.2/0.1 \pm 1.2$
FF($D^0 \rightarrow a_2(1320)^+ \pi^-$)	0.1/0.2	0.2/0.2	0.3/0.3	0.5/0.4	0.2/0.1	0.1/0.1	0.3/0.2	$0.4 \pm 0.6/0.4 \pm 0.5$
FF($D^0 \rightarrow a_2(1320)^- \pi^+$)	0.1/0.0	0.0/0.0	0.1/0.1	0.7/0.3	0.5/0.6	0.1/0.1	0.4/0.5	$0.1 \pm 1.0/0.1 \pm 0.8$
FF($D^0 \rightarrow h_1(1170)^0 \pi^0$)	-/0.7	-/0.1	-/0.2	-/1.1	-/0.7	-/0.0	-/1.0	-/0.7 ± 1.6
FF($D^0 \rightarrow \pi(1300)^+ \pi^-$)	0.6/0.9	0.1/0.1	0.0/0.0	0.9/1.0	1.1/1.2	0.2/0.1	0.6/0.2	$0.6 \pm 1.6/0.9 \pm 1.6$
FF($D^0 \rightarrow \pi(1300)^- \pi^+$)	0.1/0.4	0.2/0.2	0.0/0.1	1.1/1.4	1.2/1.5	0.1/0.1	0.5/0.1	$0.2 \pm 1.7/0.5 \pm 2.1$
FF($D^0 \rightarrow \pi(1300)^0 \pi^0$)	-/0.5	-/0.2	-/0.0	-/0.9	-/0.6	-/0.0	-/0.2	-/0.5 ± 1.1
FF($D^0 \rightarrow \pi_2(1670)^0 \pi^0$)	-/0.8	-/0.1	-/0.1	-/0.3	-/0.4	-/0.1	-/1.4	-/0.8 ± 1.5
FF($D^0 \rightarrow \rho(770)^0 \rho(770)^0$)	0.3/-	0.0/-	0.0/-	1.5/-	0.2/-	0.1/-	0.6/-	$0.3 \pm 1.6/-$
FF($D^0 \rightarrow \rho(770)^0 \rho(770)^0 [S]$)	0.1/-	0.0/-	0.1/-	0.7/-	0.3/-	0.1/-	0.3/-	$0.1 \pm 0.8/-$
FF($D^0 \rightarrow \rho(770)^0 \rho(770)^0 [P]$)	0.0/-	0.0/-	0.4/-	0.5/-	0.5/-	0.3/-	0.1/-	$0.4 \pm 0.8/-$
FF($D^0 \rightarrow \rho(770)^0 \rho(770)^0 [D]$)	0.3/-	0.0/-	0.2/-	0.9/-	0.3/-	0.1/-	0.5/-	$0.4 \pm 1.1/-$
FF($D^0 \rightarrow \rho(770)^0 \rho(1450)^0$)	0.0/-	0.0/-	0.0/-	0.7/-	0.7/-	0.1/-	0.8/-	$0.0 \pm 1.3/-$
FF($D^0 \rightarrow \rho(770)^0 \rho(1450)^0 [P]$)	0.1/-	0.2/-	0.2/-	1.3/-	0.6/-	0.3/-	0.1/-	$0.3 \pm 1.5/-$
FF($D^0 \rightarrow \rho(770)^0 \rho(1450)^0 [D]$)	0.1/-	0.1/-	0.1/-	0.2/-	0.9/-	0.1/-	0.8/-	$0.2 \pm 1.2/-$
FF($D^0 \rightarrow \rho(770)^+ \rho(770)^-$)	-/0.9	-/0.0	-/0.3	-/1.3	-/0.5	-/0.1	-/1.0	-/0.9 ± 1.7
FF($D^0 \rightarrow \rho(770)^+ \rho(770)^- [S]$)	-/0.6	-/0.1	-/0.1	-/1.1	-/0.6	-/0.0	-/1.0	-/0.6 ± 1.6
FF($D^0 \rightarrow \rho(770)^+ \rho(770)^- [P]$)	-/1.0	-/0.2	-/0.1	-/0.5	-/0.4	-/0.1	-/0.8	-/1.0 ± 1.0
FF($D^0 \rightarrow \rho(770)^+ \rho(770)^- [D]$)	-/0.1	-/0.1	-/0.2	-/0.4	-/0.3	-/0.1	-/0.6	-/0.2 ± 0.8
FF($D^0 \rightarrow \rho(770)^+ \rho(1450)^- [D]$)	-/0.7	-/0.1	-/0.4	-/1.9	-/0.8	-/0.1	-/0.7	-/0.8 ± 2.2
FF($D^0 \rightarrow \rho(770)^0 (\pi\pi)_S$)	0.5/0.3	0.0/0.0	0.2/0.2	2.7/1.8	0.1/0.1	0.0/0.0	1.0/0.7	$0.5 \pm 2.9/0.4 \pm 1.9$
FF($D^0 \rightarrow (\pi^+ \pi^-)_S (\pi\pi)_S$)	0.1/0.6	0.0/0.0	0.1/0.2	2.0/1.3	0.6/0.8	0.1/0.0	0.3/0.5	$0.1 \pm 2.1/0.6 \pm 1.6$
FF($D^0 \rightarrow f_2(1270)^0 (\pi\pi)_S$)	0.0/0.1	0.0/0.0	0.1/0.1	2.6/2.9	1.1/1.0	0.0/0.0	1.4/1.6	$0.1 \pm 3.2/0.1 \pm 3.5$
FF($D^0 \rightarrow \omega(782) \pi^0$)	-/0.1	-/0.0	-/0.1	-/0.3	-/0.1	-/0.0	-/0.4	-/0.1 ± 0.5
FF($D^0 \rightarrow \phi(1020) \pi^0$)	-/0.2	-/0.1	-/0.4	-/0.3	-/0.2	-/0.1	-/0.5	-/0.5 ± 0.6
FF($a_1(1260)^\pm \rightarrow \rho(770) \pi [S]$)	0.8/0.8	0.1/0.1	0.1/0.0	1.2/1.2	0.4/0.4	0.1/0.1	0.6/0.6	$0.8 \pm 1.4/0.8 \pm 1.4$
FF($a_1(1260)^\pm \rightarrow \rho(770) \pi [D]$)	0.1/0.1	0.0/0.0	0.2/0.2	2.2/2.1	0.5/0.4	0.0/0.0	0.1/0.1	$0.2 \pm 2.3/0.2 \pm 2.1$
FF($a_1(1260)^\pm \rightarrow f_2(1270) \pi [P]$)	0.7/0.7	0.0/0.0	0.1/0.1	0.4/0.3	1.2/1.2	0.1/0.1	0.3/0.3	$0.7 \pm 1.3/0.7 \pm 1.3$
FF($a_1(1260)^\pm \rightarrow (\pi^+ \pi^-)_S \pi [P]$)	0.8/0.9	0.1/0.0	0.2/0.2	1.0/1.6	0.3/0.1	0.2/0.1	0.9/0.8	$0.8 \pm 1.4/0.9 \pm 1.8$
FF($a_1(1260)^0 \rightarrow \rho(770) \pi [S]$)	-/0.7	-/0.1	-/0.0	-/1.4	-/0.3	-/0.1	-/0.6	-/0.7 ± 1.6
FF($a_1(1260)^0 \rightarrow \rho(770) \pi [D]$)	-/0.1	-/0.0	-/0.2	-/2.2	-/0.4	-/0.0	-/0.1	-/0.2 ± 2.2
FF($a_1(1260)^0 \rightarrow f_2(1270) \pi [P]$)	-/0.7	-/0.0	-/0.1	-/0.4	-/1.4	-/0.1	-/0.3	-/0.7 ± 1.5
FF($a_1(1260)^0 \rightarrow (\pi^+ \pi^-)_S \pi [P]$)	-/0.8	-/0.0	-/0.3	-/1.6	-/0.1	-/0.1	-/0.8	-/0.9 ± 1.8
FF($\pi(1300)^\pm \rightarrow \rho(770) \pi$)	0.0/0.2	0.1/0.1	0.3/0.3	2.0/0.8	2.2/3.3	0.1/0.1	0.4/0.3	$0.3 \pm 3.0/0.4 \pm 3.4$
FF($\pi(1300)^\pm \rightarrow (\pi^+ \pi^-)_S \pi$)	0.1/0.1	0.1/0.1	0.3/0.4	1.8/1.2	2.3/2.9	0.1/0.1	0.3/0.2	$0.3 \pm 2.9/0.4 \pm 3.1$
FF($\pi(1300)^0 \rightarrow \rho(770) \pi$)	-/0.2	-/0.1	-/0.2	-/1.0	-/3.3	-/0.1	-/0.4	-/0.3 ± 3.5
FF($\pi(1300)^0 \rightarrow (\pi^+ \pi^-)_S \pi$)	-/0.0	-/0.1	-/0.4	-/1.9	-/2.6	-/0.1	-/0.1	-/0.4 ± 3.2
$M_{a_1(1260)}$	0.5	0.1	0.0	4.0	1.2	0.1	1.6	0.5 ± 4.5
$\Gamma_{a_1(1260)}$	1.7	0.2	0.0	3.2	2.3	0.4	1.7	1.7 ± 4.3
$M_{\pi(1300)}$	0.8	0.1	0.0	1.1	1.1	0.0	1.0	0.8 ± 1.8
$\Gamma_{\pi(1300)}$	0.7	0.1	0.0	2.9	0.4	0.2	0.5	0.7 ± 3.0
F^+	0.7/1.0	0.0/0.2	0.1/0.1	0.7/0.8	0.3/0.8	0.1/0.1	1.0/0.6	$0.7 \pm 1.3/1.0 \pm 1.3$

Table 16. Branching fractions of $D^0 \rightarrow \pi^+ \pi^- \pi^+ \pi^-$ and $D^0 \rightarrow \pi^+ \pi^- \pi^0 \pi^0$ (non- η) from this work compared to the PDG [25] values, where the first uncertainties are statistical and the second are systematic.

	This work	PDG
$D^0 \rightarrow \pi^+ \pi^- \pi^+ \pi^-$	$(0.688 \pm 0.010 \pm 0.010)\%$	$(0.756 \pm 0.020)\%$
$D^0 \rightarrow \pi^+ \pi^- \pi^0 \pi^0$ (non- η)	$(0.951 \pm 0.025 \pm 0.021)\%$	$(1.005 \pm 0.090)\%$

Table 17. Branching fractions of the intermediate processes with FFs > 1% in $D^0 \rightarrow \pi^+ \pi^- \pi^+ \pi^-$ and $D^0 \rightarrow \pi^+ \pi^- \pi^0 \pi^0$. The first uncertainties are the statistical uncertainties, the second are the systematic uncertainties from the total branching fraction measurements, and the third are the systematic uncertainties of the FFs from the amplitude analysis.

Component	Branching fraction (%)	
	$\pi^+ \pi^- \pi^+ \pi^-$	$\pi^+ \pi^- \pi^0 \pi^0$
$D^0 \rightarrow a_1(1260)^+ \pi^-$	$0.566 \pm 0.024 \pm 0.008 \pm 0.110$	$0.546 \pm 0.027 \pm 0.011 \pm 0.069$
$D^0 \rightarrow a_1(1260)^- \pi^+$	$0.071 \pm 0.010 \pm 0.001 \pm 0.017$	$0.068 \pm 0.011 \pm 0.001 \pm 0.021$
$D^0 \rightarrow a_1(1260)^0 \pi^0$	—	$0.313 \pm 0.031 \pm 0.007 \pm 0.082$
$D^0 \rightarrow a_1(1640)^+ \pi^-$	$0.012 \pm 0.003 \pm 0.000 \pm 0.006$	$0.010 \pm 0.003 \pm 0.000 \pm 0.007$
$D^0 \rightarrow h_1(1170)^0 \pi^0$	—	$0.012 \pm 0.006 \pm 0.000 \pm 0.010$
$D^0 \rightarrow \pi(1300)^+ \pi^-$	$0.222 \pm 0.018 \pm 0.003 \pm 0.031$	$0.148 \pm 0.014 \pm 0.003 \pm 0.025$
$D^0 \rightarrow \pi(1300)^- \pi^+$	$0.162 \pm 0.016 \pm 0.002 \pm 0.028$	$0.108 \pm 0.011 \pm 0.002 \pm 0.021$
$D^0 \rightarrow \pi(1300)^0 \pi^0$	—	$0.221 \pm 0.027 \pm 0.005 \pm 0.033$
$D^0 \rightarrow \pi_2(1670)^0 \pi^0$	—	$0.010 \pm 0.002 \pm 0.000 \pm 0.004$
$D^0 \rightarrow \rho(770)^0 \rho(770)^0$	$0.193 \pm 0.013 \pm 0.003 \pm 0.022$	—
$D^0 \rightarrow \rho(770)^0 \rho(770)^0 [S]$	$0.012 \pm 0.004 \pm 0.000 \pm 0.003$	—
$D^0 \rightarrow \rho(770)^0 \rho(770)^0 [P]$	$0.067 \pm 0.007 \pm 0.001 \pm 0.006$	—
$D^0 \rightarrow \rho(770)^0 \rho(770)^0 [D]$	$0.159 \pm 0.015 \pm 0.002 \pm 0.017$	—
$D^0 \rightarrow \rho(770)^0 \rho(1450)^0$	$0.017 \pm 0.006 \pm 0.000 \pm 0.008$	—
$D^0 \rightarrow \rho(770)^0 \rho(1450)^0 [P]$	$0.007 \pm 0.003 \pm 0.000 \pm 0.003$	—
$D^0 \rightarrow \rho(770)^0 \rho(1450)^0 [D]$	$0.010 \pm 0.006 \pm 0.000 \pm 0.008$	—
$D^0 \rightarrow \rho(770)^+ \rho(770)^-$	—	$0.864 \pm 0.040 \pm 0.018 \pm 0.075$
$D^0 \rightarrow \rho(770)^+ \rho(770)^- [S]$	—	$0.124 \pm 0.019 \pm 0.003 \pm 0.033$
$D^0 \rightarrow \rho(770)^+ \rho(770)^- [P]$	—	$0.186 \pm 0.013 \pm 0.004 \pm 0.019$
$D^0 \rightarrow \rho(770)^+ \rho(770)^- [D]$	—	$0.342 \pm 0.029 \pm 0.007 \pm 0.024$
$D^0 \rightarrow \rho(770)^+ \rho(1450)^- [D]$	—	$0.016 \pm 0.008 \pm 0.000 \pm 0.016$
$D^0 \rightarrow \rho(770)^0 (\pi\pi)_S$	$0.019 \pm 0.004 \pm 0.000 \pm 0.012$	$0.010 \pm 0.002 \pm 0.000 \pm 0.004$
$D^0 \rightarrow (\pi^+ \pi^-)_S (\pi\pi)_S$	$0.432 \pm 0.032 \pm 0.006 \pm 0.066$	$0.356 \pm 0.029 \pm 0.007 \pm 0.049$
$D^0 \rightarrow f_2(1270)^0 (\pi\pi)_S$	$0.012 \pm 0.003 \pm 0.000 \pm 0.008$	$0.010 \pm 0.002 \pm 0.000 \pm 0.008$
$D^0 \rightarrow \omega(782) \pi^0$	—	$0.009 \pm 0.004 \pm 0.000 \pm 0.002$
$D^0 \rightarrow \phi(1020) \pi^0$	—	$0.014 \pm 0.004 \pm 0.000 \pm 0.003$

sample is smeared by a Gaussian function, while the mean and width are obtained by performing a fit to the ΔE distribution of the data with the signal MC shape convolved with a Gaussian function. The resultant changes of the efficiencies with respect to the nominal values, 0.1% for both $D^0 \rightarrow \pi^+ \pi^- \pi^+ \pi^-$ and $D^0 \rightarrow \pi^+ \pi^- \pi^0 \pi^0$, are taken as the systematic uncertainties.

• ST fit

The systematic uncertainty of the ST fit is studied by changing the signal and background shapes. The signal shape is changed by replacing the Gaussian resolution with a Crystal Ball function [57]. The background shape is changed with a floating cut-off parameter for the ARGUS function. The square root of the quadrature sum of the relative change of the ST yields, which gives 0.5%, is

Table 18. Relative systematic uncertainties (%) of the measured branching fractions.

Source	$\mathcal{B}(D^0 \rightarrow \pi^+\pi^-\pi^+\pi^-)$	$\mathcal{B}(D^0 \rightarrow \pi^+\pi^-\pi^0\pi^0)$
π^\pm tracking	0.4	0.2
π^\pm PID	1.2	0.6
π^0 reconstruction	-	1.3
ΔE cut in signal side	0.1	0.1
ST fit	0.5	0.5
DT fit	0.6	1.4
Amplitude model	0.3	0.6
Quantum correlation correction	0.3	0.4
MC statistics	0.1	0.2
Total	1.5	2.2

taken as the systematic uncertainty.

• DT fit

As described in Sec. VII, the systematic uncertainties of the DT fit are obtained by varying the signal and background shapes and the yields of the peaking backgrounds in BKGVI in the fit. The square roots of the quadrature sums of the relative changes of the DT yields in the individual changes are 0.6% and 1.4% for $D^0 \rightarrow \pi^+\pi^-\pi^+\pi^-$ and $D^0 \rightarrow \pi^+\pi^-\pi^0\pi^0$, respectively, which are taken as the systematic uncertainties.

• Amplitude model

The DT efficiencies are obtained by varying the parameters of the amplitude model within their uncertainties. The resultant standard deviations of the DT efficiencies, which are 0.3% and 0.6% for $D^0 \rightarrow \pi^+\pi^-\pi^+\pi^-$ and $D^0 \rightarrow \pi^+\pi^-\pi^0\pi^0$, respectively, are taken as the systematic uncertainties.

• Quantum correlation corrections

The uncertainties associated with the input parameters of quantum correlation (r , R , δ , and F_+) are 0.3% and

0.4% for $D^0 \rightarrow \pi^+\pi^-\pi^+\pi^-$ and $D^0 \rightarrow \pi^+\pi^-\pi^0\pi^0$, respectively, which are assigned according to uncertainty propagation.

• MC statistics

The systematic uncertainties related with the limited statistics of the signal MC samples are 0.1% and 0.2% for $D^0 \rightarrow \pi^+\pi^-\pi^+\pi^-$ and $D^0 \rightarrow \pi^+\pi^-\pi^0\pi^0$, respectively.

IX. SUMMARY

Using 2.93 fb^{-1} of the e^+e^- collision data taken at $\sqrt{s} = 3.773 \text{ GeV}$ with the BESIII detector, a joint amplitude analysis of $D^0 \rightarrow \pi^+\pi^-\pi^+\pi^-$ and $D^0 \rightarrow \pi^+\pi^-\pi^0\pi^0$ (non- η) is performed. Large interferences between the dominant amplitudes of $D^0 \rightarrow a_1(1260)\pi$, $D^0 \rightarrow \pi(1300)\pi$, $D^0 \rightarrow \rho(770)\rho(770)$, and $D^0 \rightarrow 2(\pi\pi)_S$ are observed. Based on the amplitude model, the model dependent CP -even fractions of $D^0 \rightarrow \pi^+\pi^-\pi^+\pi^-$ and $D^0 \rightarrow \pi^+\pi^-\pi^0\pi^0$ (non- η) are determined to be $(75.2 \pm 1.1_{\text{stat.}} \pm 1.5_{\text{syst.}}) \%$ and $(68.9 \pm 1.5_{\text{stat.}} \pm 2.4_{\text{syst.}}) \%$, respectively, consistent with the previous measurements performed by the CLEO [6, 13, 52] and BESIII [53, 54] collaboration. The branching fractions of $D^0 \rightarrow \pi^+\pi^-\pi^+\pi^-$ and $D^0 \rightarrow \pi^+\pi^-\pi^0\pi^0$ (non- η) are measured to be $(0.688 \pm 0.010_{\text{stat.}} \pm 0.010_{\text{syst.}}) \%$ and $(0.951 \pm 0.025_{\text{stat.}} \pm 0.021_{\text{syst.}}) \%$, respectively, where the former is 3σ lower than the PDG [25] value. This 3σ deviation may be due to amplitude model variations, which affect the global reconstruction efficiency. These results provide essential information to the search for CP violation [9] and measurements of the binned strong phase parameter [6], which are important inputs in the γ measurement via the $B^- \rightarrow DK^-$ decay.

ACKNOWLEDGEMENTS

The BESIII Collaboration thanks the staff of BEPCII, the IHEP Computing Center, and the Supercomputing Center of the University of Science and Technology of China (USTC) for their immense support.

References

- [1] N. Cabibbo, *Phys. Rev. Lett.* **10**, 531 (1963)
- [2] M. Kobayashi and T. Maskawa, *Prog. Theor. Phys.* **49**, 652 (1973)
- [3] M. Gronau and D. Wyler, *Phys. Lett. B* **265**, 172 (1991)
- [4] D. Atwood, I. Dunietz, and A. Soni, *Phys. Rev. Lett.* **78**, 3257 (1997)
- [5] A. Giri, Y. Grossman, A. Soffer *et al.*, *Phys. Rev. D* **68**, 054018 (2003)
- [6] S. Harnew, P. Naik, C. Prouve *et al.*, *JHEP* **01**, 144 (2018)
- [7] R. Aaij *et al.* (The LHCb collaboration), *JHEP* **08**, 041 (2019)
- [8] A. Poluektov *et al.*, *Phys. Rev. D* **70**, 072003 (2004)
- [9] R. Aaij *et al.*, *Phys. Lett. B* **769**, 345 (2017)
- [10] H. Y. Cheng, *Phys. Rev. D* **67**, 094007 (2003)
- [11] H. Y. Cheng and C. W. Chiang, *Phys. Rev. D* **81**, 074021 (2010)
- [12] J. M. Link *et al.*, *Phys. Rev. D* **75**, 052003 (2007)
- [13] P. d'Argent, N. Skidmore *et al.*, *JHEP* **05**, 143 (2017)
- [14] R. M. Baltrusaitis *et al.*, *Phys. Rev. Lett.* **56**, 2140 (1986)
- [15] H. B. Li and X. R. Lyu, *Natl. Sci. Rev.* **8**, nwab181 (2021)
- [16] M. Ablikim *et al.*, *Nucl. Instrum. Meth. A* **614**, 345 (2010)
- [17] C. Yu *et al.*, BEPC II Performance and Beam Dynamics Studies on Luminosity, in *7th International Particle Accelerator Conference*, page TUYA01, 2016.
- [18] M. Ablikim *et al.*, *Chin. Phys. C* **44**, 040001 (2020)
- [19] S. Agostinelli *et al.*, *Nucl. Instrum. Meth. A* **506**, 250

- (2003)
- [20] K. X. Huang *et al.*, *Nucl. Sci. Tech.* **33**, 142 (2022)
- [21] S. Jadach, B. F. L. Ward, and Z. Was, *Phys. Rev. D* **63**, 113009 (2001)
- [22] S. Jadach, B. F. L. Ward, and Z. Was, *Comput. Phys. Commun.* **130**, 260 (2000)
- [23] D. J. Lange, *Nucl. Instrum. Meth. A* **462**, 152 (2001)
- [24] R. G. Ping, *Chin. Phys. C* **32**, 599 (2008)
- [25] R. L. Workman *et al.*, *PTEP* **2022**, 083C01 (2022)
- [26] J. C. Chen, G. S. Huang, X. R. Qi *et al.*, *Phys. Rev. D* **62**, 034003 (2000)
- [27] R. L. Yang, R. G. Ping, and H. Chen, *Chin. Phys. Lett.* **31**, 061301 (2014)
- [28] E. Richter-Was, *Phys. Lett. B* **303**, 163 (1993)
- [29] M. Ablikim *et al.*, *Phys. Lett. B* **734**, 227 (2014)
- [30] H. Albrecht *et al.*, *Phys. Lett. B* **241**, 278 (1990)
- [31] Y. S. Amhis *et al.*, *Eur. Phys. J. C* **81**, 226 (2021)
- [32] M. Ablikim *et al.*, *JHEP* **05**, 164 (2021)
- [33] N. Berger, B. Liu, and J. Wang, *J. Phys. Conf. Ser.* **219**, 042031 (2010)
- [34] F. Von Hippel and C. Quigg, *Phys. Rev. D* **5**, 624 (1972)
- [35] S. Mandelstam, J. E. Paton, R. F. Peierls *et al.*, *Annals Phys.* **18**, 198 (1962)
- [36] D. Herndon, P. Soding, and R. J. Cashmore, *Phys. Rev. D* **11**, 3165 (1975)
- [37] J. J. Brehm, *Annals Phys.* **108**, 454 (1977)
- [38] W. Rarita and J. Schwinger, *Phys. Rev.* **60**, 61 (1941)
- [39] C. Zemach, *Phys. Rev.* **140**, B97 (1965)
- [40] S. U. Chung, *Phys. Rev. D* **57**, 431 (1998)
- [41] B. S. Zou and D. V. Bugg, *Eur. Phys. J. A* **16**, 537 (2003)
- [42] G. J. Gounaris and J. J. Sakurai, *Phys. Rev. Lett.* **21**, 244 (1968)
- [43] M. Ablikim *et al.*, *Phys. Lett. B* **607**, 243 (2005)
- [44] V. V. Anisovich and A. V. Sarantsev, *Eur. Phys. J. A* **16**, 229 (2003)
- [45] B. Aubert *et al.*, *Phys. Rev. D* **78**, 034023 (2008)
- [46] G. D. Alexeev *et al.*, *Phys. Rev. Lett.* **127**, 082501 (2021)
- [47] M. Aghasyan *et al.*, *Phys. Rev. D* **98**, 092003 (2018)
- [48] M. Pivk and F. R. Le Diberder, *Nucl. Instrum. Meth. A* **555**, 356 (2005)
- [49] F. James and M. Roos, *Comput. Phys. Commun.* **10**, 343 (1975)
- [50] B. Efron, *The Annals of Statistics* **7**, 1 (1979)
- [51] C. Langenbruch, *Eur. Phys. J. C* **82**, 393 (2022)
- [52] S. Malde *et al.*, *Phys. Lett. B* **747**, 9 (2015)
- [53] M. Ablikim *et al.*, *Phys. Rev. D* **106**, 092004 (2022)
- [54] M. Ablikim *et al.*, *Phys. Rev. D* **106**, 092005 (2022)
- [55] M. Ablikim *et al.*, *Phys. Rev. D* **97**, 072004 (2018)
- [56] D. V. Bugg, *J. Phys. G* **34**, 151 (2007)
- [57] T. kwarnicki, *A study of the radiative CASCADE transitions between the Upsilon-Prime and Upsilon resonances*, PhD thesis, Cracow, INP, 1986.